Dendritic Peptide Release Mediates Interpopulation Crosstalk between Neurosecretory and Preautonomic Networks

Please cite this article as: Son, SJ, Filosa, JA, Potapenko, ES, Biancardi, VC, Zheng, H, Patel, KP, Tobin, VA, Ludwig, M & Stern, JE, 'Dendritic Peptide Release Mediates Interpopulation Crosstalk between Neurosecretory and Preautonomic Networks' Neuron 2013, http://dx.doi.org/10.1016/j.neuron.2013.04.025

DENDRITIC PEPTIDE RELEASE MEDIATES INTER-POPULATION CROSSTALK BETWEEN NEUROSECRETORY AND PREAUTONOMIC NETWORKS

Son, SJ[1], Filosa JA[1], Potapenko[1], E; Biancardi[1], VC, Zheng H[2], Patel KP[2], Tobin VA[3] Ludwig M[3], and Stern JE[1]

[1]Department of Physiology, Georgia Health Sciences University, Augusta GA USA

[2]Department of Cellular and Integrative Physiology, University of Nebraska Medical Center, Omaha, Nebraska

[3]Centre for Integrative Physiology, University of Edinburgh, Edinburgh UK

Running Title: Neurosecretory-autonomic interpopulation crosstalk

Corresponding Author

Javier E. Stern, M.D., Ph.D.

Department of Physiology

Georgia Health Sciences University

1120 15th St. Augusta GA USA

jstern@georgiahealth.edu

Phone: 706-721-2180

Fax: 706-721-7299

Highlights

- Proof of a novel signaling modality mediating inter-population crosstalk in the brain
- Dendritic VP release from neurosecretory neurons stimulates autonomic neurons
- Crosstalk involves Ca^{2+}-mediated activation of a CAN channel in autonomic neurons
- This crosstalk is involved in the generation of polymodal homeostatic responses

SUMMARY

While communication between neurons is classically considered a function of the synapse, neurons can also release neurotransmitter from their dendrites. We found that dendritic transmitter release coordinates activity across distinct neuronal populations to generate integrative homeostatic physiological responses. We show that activity-dependent release of vasopressin from hypothalamic neuroendocrine neurons in the paraventricular nucleus stimulates neighboring (~100 μm soma-to-soma) presympathetic neurons, resulting in a sympathoexcitatory population response. This inter-population crosstalk was engaged by an NMDA-mediated increase in dendritic Ca^{2+}, was influenced by vasopressin's ability to diffuse in the extracellular space, and involved activation of CAN channels at the target neurons. Furthermore, we demonstrate that this inter-population crosstalk plays a pivotal role in the generation of a systemic, polymodal neurohumoral homeostatic response to a hyperosmotic challenge. Since dendritic release is emerging as a widespread process, our results suggest that a similar mechanism could mediate inter-population crosstalk in other brain systems, particularly those involved in generating complex behaviors.

INTRODUCTION

Information processing in the CNS involves a wide array of spatiotemporal scales, ranging from temporally fast and spatially precise (critical for coherent spike timing between two neurons (Galarreta and Hestrin, 2001), to temporally slow and spatially diffuse, a modality best-suited for the coordination of activity within or across entire neuronal populations (Fuxe et al., 2007; Leng and Ludwig, 2008). Despite the importance of the latter in the generation of complex behaviors (Ludwig and Leng, 2006), the precise signaling mechanisms underlying inter-population crosstalk in the brain remain largely unknown.

Neuropeptides are increasingly recognized as unique signals involved in information processing in the brain (Leng and Ludwig, 2008; Salio et al., 2006). They are abundantly found in dendrites (Guan et al., 2005; Pow and Morris, 1989), their release is generally not confined to, or targeted at synaptic/postsynaptic sites, and given their relatively long half-lives (Mens et al., 1983), they can diffuse in the extracellular space (ECS) to act on distant targets. Thus, unlike classical fast-acting neurotransmitters, neuropeptide signaling lacks temporal and spatial precision, making it ideally suited to mediate communication between populations of neurons (Fuxe et al., 2007; Landgraf and Neumann, 2004; Ludwig and Leng, 2006).

Neuropeptides are widely used as signaling molecules in the hypothalamus, particularly within the supraoptic (SON) and paraventricular (PVN) nuclei. These centers are critically involved in the generation of complex polymodal homeostatic responses, consisting of orchestrated activities of autonomic and neuroendocrine networks (Buijs and Van Eden, 2000; Swanson and Sawchenko, 1980). During disturbances of fluid/electrolyte homeostasis, activation of magnocellular neurosecretory (MNNs) and presympathetic neurons in the PVN results in the concerted systemic release of the hormone vasopressin (VP), along with an increase in renal sympathetic outflow, respectively, acting together to restore fluid/electrolyte balance (Bourque, 2008; Toney and Stocker, 2010). Importantly, an imbalanced interaction amongst these systems results in maladaptive responses characteristic of disease conditions, including stress, and hypertension (Ely, 1995; Esler et al., 1995). Thus, generation of homeostatic

responses by the PVN represents an ideal paradigm to study inter-population signaling mechanisms within the brain, both under physiological and pathological conditions.

In addition to playing key roles in the processing and integration of synaptic inputs, dendrites are recognized to be major sources of brain neuropeptides (Guan et al., 2005; Pow and Morris, 1989), MNNs being one of the best-studied prototypes of dendritic peptide release (Ludwig and Leng, 2006). Besides releasing their peptide content from neurohypophyseal axonal terminals into the circulation, MNNs also release VP and oxytocin (OT) locally from their dendrites, serving as a powerful autocrine signal by which they auto-regulate their activity (Gouzenes et al., 1998; Ludwig and Leng, 1997). However, whether dendritically released peptides from MNNs can act beyond their own secreting population, to mediate inter-population crosstalk, has not yet being explored. Using the magnocellular neurosecretory system as a unique model system, we tested the hypothesis that dendritic peptide release constitutes a powerful inter-population signaling modality in the brain. More specifically, we assessed whether dendritically released VP mediates crosstalk between neurosecretory and presympathetic hypothalamic neurons in the context of homeostatic neurohumoral responses to an osmotic challenge.

Using a combination of *in vitro* approaches in acute hypothalamic slices, including patch-clamp electrophysiology, confocal imaging and laser photolysis of caged molecules, we demonstrate that dendritically-released VP from a single stimulated neurosecretory neuron evoked a direct excitatory response in presympathetic neurons located ~100 μm away. Moreover, we found that activity-dependent dendritic VP release from the whole population of neurosecretory neurons translated into a diffusible pool of peptide that tonically stimulated presympathetic neuronal activity. Finally, using an *in vivo* homeostatic challenge, we show that dendritic VP release is critical for the recruitment of presympathetic neurons, resulting in an optimal sympathoexcitatory outflow during a homeostatic challenge that requires an orchestrated neurosecretory and sympathetic response.

RESULTS

Intimate dendro-somatic and dendro-dendritic interrelationships between presympathetic and magnocellular neurosecretory PVN neurons.

It is well-documented that neurosecretory and presympathetic neuronal somata in the PVN are anatomically compartmentalized within specific subnuclei (Swanson and Kuypers, 1980; Swanson and Sawchenko, 1980). Using a combination of retrograde tract tracing and immunohistochemistry to identify presympathetic PVN neurons that innervate the rostroventrolateral medulla (RVLM; PVN-RVLM neurons) and VP MNNs, respectively, we verified this early observation (***Fig.1A***). However, a more detailed analysis revealed that thick and varicose dendritic processes from VP MNNs extended beyond their own neuronal compartment, coming in close proximity to somatodendritic elements of presympathetic neurons in the ventromedial, dorsal cap and posterior parvocellular subnuclei (Swanson and Kuypers, 1980) (***Fig.1B-G***). The identity of these processes as dendrites was confirmed by MAP2 immunoreactivity (***Fig.1I***), and by being abutted by numerous dopamine β hydroxylase (DBH)-immunoreactive presynaptic boutons (***Fig.1J*).** Conversely, VP axons ran laterally out of the PVN boundaries, then turning ventrally and caudally towards the median eminence (***Fig.1H*)** (Swanson and Kuypers, 1980). These studies support thus a distinctive anatomical microenvironment that would enable dendro-dendritic/somatic communication from neurosecretory to presympathetic neurons, possibly via dendritically released VP.

Activation of V1a receptors in presympathetic PVN neurons increases their firing activity via a Ca^{2+}-dependent activation of TRPM4/5 channels.

To determine if presympathetic neurons sense dendritically-released VP from MNNs, we first assessed for the expression of V1a receptors (the most common type of VP receptor found in the brain (Zingg, 1996)) in retrogradely-labeled PVN-RVLM neurons. As shown in ***Fig.2A-D,*** we found a dense V1a receptor immunoreactivity in somato-dendritic regions of presympathetic neurons. Similar results were found with an alternative V1a antibody (***Fig.S1),*** recently shown to label V1a receptors in olfactory bulb neurons (Tobin et al., 2010). The resolution of the light microscopic approach however, does not readily distinguish V1a clusters located near the surface membrane of PVN-RVLM neurons from ones potentially located at presynaptic terminals. Further

supporting the expression of V1a receptors by PVN-RVLM neurons, however, we report expression of V1a receptor mRNA in these neuronal population (***Fig.2E***).

Focal application of VP onto presympathetic PVN neurons resulted in direct membrane depolarization and increased firing discharge (n=16, P<0.001, ***Fig.2F-I).*** VP effects were almost completely blocked by a selective V1a receptor antagonist (β-Mercapto-β,β-cyclopentamethylenepropionyl[1], O-me-Tyr[2], Arg[8]]-Vasopressin, 1 μM, P< 0.01, n=8, ***Fig.2H***), but persisted in the presence of the ionotropic glutamate and $GABA_A$ receptor antagonists kynurenate (1 mM) and bicucculine (20 μM)(basal: 0.30 ± 0.13 Hz; VP: 2.75 ± 0.53 Hz, P<0.01, n=6), or in the presence of a low Ca^{2+} synaptic block media (basal: 0.58 ± 0.38 Hz; VP: 3.85 ± 0.38 Hz, P< 0.02).

The VP-mediated increase in firing activity in presympathetic neurons was preceded (3.1 ± 0.8 s) by an increase in $[Ca^{2+}]_I$ (P< 0.01, n=8, ***Fig.3A-C***), and was abolished by chelation of intracellular Ca^{2+} with BAPTA (10 mM) (n=8, ***Fig.3D)***. In voltage-clamp mode, VP evoked an outwardly rectifying current with an apparent reversal potential of ~ -15 mV (***Fig.3E)***. Taken together, these results support the involvement of a Ca^{2+}-activated non-selective cation current (CAN) (Petersen, 2002). We found PVN-RVLM neurons to express dense immunoreactivity (***Fig.S2A-D***) and mRNA (***Fig.S2E)*** for TRPM4 channels, a major CAN channel member of the transient receptor potential (TRP) family (Ullrich et al., 2005), and previously reported in the hypothalamus (Ghamari-Langroudi and Bourque, 2002; Teruyama and Armstrong, 2007; Teruyama et al., 2011). We also found that VP excitatory effects on PVN-RVLM neurons were blocked by flufenamic acid (FFA, 200 μM) (n=9, ***Fig.S2F***), a relatively specific blocker of TRPM4/5 channels (Ullrich et al., 2005). In the presence of FFA, PVN-RVLM neurons were still capable of displaying a burst of action potential in response to a puff of 20 μM NMDA (n=3, *not shown*), indicating that FFA effects were not due to non-specific effects on overall neuronal function, or due to changes in PVN-RVLM responsiveness to NMDA. Further studies however, are needed to precisely identify the molecular identity of the CAN channel underlying VP actions in presympathetic neurons.

Dendritic release of vasopressin mediates cell-cell communication between neighboring neurosecretory and presympathtic neurons.

To directly probe for a crosstalk between MNNs and presympathetic neurons, we developed an approach using transgenic eGFP-VP rats (Ueta et al., 2005) that received an injection of a fluorescent retrograde tracer in the RVLM (***Fig.S3)***. Our approach consisted on selectively activating individual VP neurons using laser photolysis of caged-NMDA, while simultaneously monitoring the electrical activity of neighboring presympathetic neurons in acute hypothalamic slices. To validate this approach, we show that laser photolysis of caged-NMDA onto restricted somatodendritic regions of patched eGFP-VP neurosecretory neurons induced reproducible inward currents along with a concurrent high-frequency burst of action potentials (***Fig.4A)***, previously shown to efficiently evoke dendritic release of peptides from MNNs in brain slices (Kombian et al., 1997). Moreover, photolysis of caged-NMDA in the somata of Fluo-5F loaded eGFP-VP neurons increased $[Ca^{2+}]_i$ levels, which rapidly propagated into dendritic compartments (***Fig.S4)***.

To test the hypothesis that dendritic VP release acts as a crosstalk signal between neurosecretory and presympathetic neurons, we then obtained patch recordings from PVN-RVLM neurons, and assessed their responses to photolysis of caged-NMDA in neighboring eGFP-VP neurons. On average, 3 different eGFP-VP neurons were photoactivated *per* patched PVN-RVLM neuron. The mean distance between the somata of presympathetic and the photoactivated VP neurons was 111.6±7.9 μm. Photolysis of caged-NMDA at the somata of individual eGFP-VP neurons consistently evoked an excitatory response in neighboring PVN-RVLM neurons, characterized by a burst of activity, which was underlain by a membrane depolarization (n=38 eGFP-VP neurons/11 PVN-RVLM neurons, $P< 0.001$, ***Fig.4B)***. Responses in presympathetic neurons occurred with a mean latency of 3.5 ± 1.0 sec following photolysis in neighboring eGFP-VP neurons. In a few cases (n=4), stimulation of an eGFP-VP neuron failed to evoke a response in PVN-RVLM neurons, which were however responsive to other eGFP-VP neurons in the same preparation.

Direct photolysis of caged-NMDA onto the recorded neurons (eGFP-VP or presympathetic) resulted in an almost instantaneous effect ($P< 0.05$ n=11, ***Fig.4)***. Importantly, presympathetic responses to photoactivation of eGFP-VP neurons were almost completely blocked following bath application of the V1a receptor antagonist

Fig.4C). No relationship between the uncaging distance and magnitude or delay of the evoked response was observed.

While action potentials are necessary for axonal VP release, dendritic release can occur in Ca^{2+}-dependent, but action potential-independent manner (Ludwig et al., 2002). Thus, to rule out a potential, but unlikely contribution of VP released from an axon collateral within the PVN (Hatton et al., 1985; Ludwig, 1998), experiments were repeated in the presence of 1 μM TTX. Under these conditions, photolysis of NMDA onto eGFP-VP neurons still evoked a membrane depolarization in neighboring PVN-RVLM neurons (n=18), effects that were blocked by the V1a receptor antagonist ($P< 0.01$, n=14, ***Fig.5***). Conversely, following activation of eGFP-VP neurons, presympathetic responses were prevented by a 0 Ca^{2+} / 3 mM EGTA aCSF (Δ 1.2 ± 0.2 mV, n=10, $P> 0.3$), without altering PVN-RVLM responses to direct uncaging of NMDA (Δ 5.5 ± 0.5 mV, $P< 0.05$ n=4). These results support that Ca^{2+}-dependent dendritic release of VP (Ludwig et al., 2002) stimulates the activity of neighboring presympathetic PVN neurons via activation of V1a receptors.

To rule out the possibility that PVN-RVLM neuronal responses were due to diffusion of caged-NMDA beyond the photoactivated region in the eGFP-VP neurons, a subset of recorded PVN-RVLM neurons were dialysed with the NMDAR blocker MK-801 (1 mM). While intracellular MK801 significantly blocked the effect of direct photolysis of caged-NMDA onto the recorded neurons (Δ 1.3 ± 0.9 mV, $P> 0.2$, n=4), photolysis onto eGFP-VP neurons still evoked a depolarizing response from the same PVN-RVLM neurons (Δ 5.2 ± 1.4 mV, $P< 0.05$, n=4) (***Fig.S5***). Additional controls included laser stimulation without the presence of caged-NMDA, and bath application of caged-NMDA alone, both of which failed to evoke neuronal responses (*not shown*)**.** Finally, NMDA uncaging onto eGFP-VP neurons (n=33) failed to evoke changes in $[Ca^{2+}]_I$ in the vast majority of Rhod-2 loaded astrocytes (~87%). In the few responsive astrocytes, increases in $[Ca^{2+}]_I$ occurred with a long delay (> 40 s) (***Fig.S6***).

To further prove the neurosecretory-presympathetic neuronal crosstalk, we performed dual-patch recordings from identified eGFP-VP and PVN-RVLM neurons. In 13/15 pairs tested, we found that evoked bursting firing in VP neurons resulted in a significant membrane depolarization ($P< 0.001$, n=13) and increase firing discharge (P<

0.02, n=13) in the neighboring presympathetic neurons ***(Fig.6B,F)***. These effects were largely blocked following bath application of the V1a antagonist (n=7) or in pairs in which eGFP-VP neurons were dialyzed with BAPTA (n=5) (***Fig.6C,F***). No responses were observed in the remaining two pairs. We found that the latency for the evoked PVN-RVLM depolarization was significantly longer when a prominent after-hyperpolarizing potential (AHP) following the evoked bursts of action potentials was observed in the paired eGFP-VP neuron (n=9, ***Fig.6B1***), compared to neurons in which AHPs were absent (n=6, ***Fig.6B2),*** or those in which a depolarizing afterpotential (DAP) was observed instead (n=3; ***Fig.6D***) ($P<0.001$, ***Fig.6E***). Moreover, a significant correlation between the eGFP-VP AHP duration and the PVN-RVLM latency was found (Pearson $r= 0.89$, $P< 0.0001$). The mean latency in paired recordings in which AHPs in eGFP-VP neurons were absent was similar to that observed following photolysis of caged NMDA ($P> 0.3$, see above), in which AHPs were not observed. In contrast to the effect on latency, the magnitude of the PVN-RVLM response was independent of the presence or duration of an AHP in the stimulated eGFP-VP neurons (not shown).

Finally, to determine whether astrocytes participate as intermediaries in the neurosecretory-presympathetic crosstalk, experiments were repeated following functional ablation of astrocytes with the selective gliotoxin L-aminoadipic acid (L-AAA, 250 μM, 30-60 min)(McBean, 1994; Xu et al., 2008). Under this condition, stimulation of eGFP-VP neurons still efficiently evoked an excitatory response in PVN-RVLM neurons ($P< 0.001$, n=5, (***Fig.6D,F***).

In a few cases (n=4) in which both neurons where intracellularly labeled with fluorescent dyes, segments of dendrites from the paired neurons were found in close proximity (12.5 ± 3.1 μm) (***Fig.6G1-G3***).

An activity-dependent diffusible VP pool tonically stimulates presympathetic neuronal activity.

Our results demonstrate that evoked dendritic peptide release from an individual VP neuron can diffuse locally to affect the activity of a neighboring presympathetic neuron. We then tested whether the basal average activity of the neurosecretory VP population as a whole was sufficient to generate a tonic diffusing peptide pool, to continuously modulate presympathetic neuronal activity. Blockade of V1a receptors *per se* resulted in

membrane hyperpolarization and inhibition of firing activity in presympathetic neurons ($P< 0.001$ and $P< 0.01$, respectively, n=14, ***Fig.7A,B***), unveiling the presence of a diffusible, tonic pool of VP. Conversely, the firing activity of eGFP-VP neurons was not affected (baseline: 2.2 ± 0.6 Hz; V1a antagonist: 2.2 ± 0.7 Hz, n=5). To test whether the strength of the diffusible pool was dependent on the degree of activity of the VP population, we performed manipulations that either increased or decreased VP neuronal activity. The VP tone was enhanced by increasing extracellular K^+ concentration (8.0 mM K^+), as indicated by a more pronounced effect of the V1a antagonist in this condition, compared to normal K^+ ACSF ($P< 0.01$, ***Fig. 7D***). Conversely, in the presence of the κ opiod receptor agonist U-50488 (1 μM), known to strongly inhibit VP neuronal activity ($P< 0.01$, ***Fig.S7A***, see also (Brown et al., 1998)), the V1a antagonist effect on presympatehtic neuronal activity was significantly blunted ($P< 0.05$ vs. control, ***Fig.7C,D***). In the presence of the V1a antagonist, however, U-50488 failed to affect the firing activity of presympathetic neurons ($P> 0.6$, n=4, ***Fig.S7B)***, arguing against a direct effect of U50488 on the latter. No correlation between basal PVN-RVLM firing activity and the magnitude of the V1a antagonist effect was found in any of these different conditions (Pearson *r* value: -0.02, $P> 0.5$). Dialysis of BAPTA into the recorded PVN-RVLM neurons prevented the effects of the V1a antagonist (baseline: 0.7 ± 0.1 Hz; V1a antagonist: 0.6 ± 0.1 Hz, $P>0.3$, n=6).

A diffusible signal in the ECS could be influenced both by its half-life and the ECS tortuosity. Blockade of tissue aminopeptidase activity (amastatin 10 μM), increased the firing activity of presympathetic neurons ($P< 0.01$, n=8, ***Fig.7E***). The amastatin effect was not only blocked, but actually turned into an inhibitory effect in the presence of the V1a receptor blocker ($P< 0.01$ *vs.* amastatin control, n=7, ***Fig.7E)***. These results indicate that aminopeptidase blockade increased not only the availability and excitatory actions of endogenous VP, but also of an unknown inhibitory signal, which was only unmasked when the VP excitatory effect was blocked. The identity of this inhibitory peptide signal was not further investigated in this study.

Reducing the coefficient of diffusion in the ECS with 5% dextran (40 kDA) (Min et al., 1998; Piet et al., 2004) also blocked the V1a antagonist effect on presympathetic firing discharge (-6.5 ± 8.8%, $P> 0.6$, n=4). Taken together, these results indicate that

tonically released VP within the PVN serves as a neurosecretory population signal, which acting in a diffusible manner, increased the activity of the presympathetic PVN neuronal population.

Dendritic release of VP within the PVN contributes to the recruitment of sympathetic neurons during an osmotic challenge.

We finally assessed whether dendritic release of VP serves as an inter-population signal by which the integrated sympathoexcitatory output from the entire presympathetic neuronal population was modulated. To this end, we performed *in vivo* studies to directly monitor sympathoexcitatory outflow from the PVN. We found that direct microinjection of VP (8-32 pmol) onto the PVN elicited a dose-dependent sympathoexcitatory response, reflected by an increase in renal sympathetic nerve activity (RSNA, $P< 0.02$, n=9, ***Fig.8A,B***). These results indicate that the VP excitatory effect observed on presympathetic neurons *in vitro* translated into a systemic, population sympathoexcitatory response.

It is well-documented that a central osmotic challenge results in a robust PVN homeostatic response that involves an orchestrated activation of VP MNNs and presympathetic neurons, leading to increased plasma VP levels along with a concomitant increase in sympathetic outflow (Bourque, 2008; Toney and Stocker, 2010), respectively. Thus, we used this paradigm to assess the functional relevance of the neurosecretory-presympathetic crosstalk in the context of a homeostatic challenge. Intra-carotid infusions of graded concentrations of NaCl (0.3, 0.9 and 2.1 osmol/l) induced a significant and dose-dependent increase in RSNA ($P<0.0001$, n=7, ***Fig.8C,D***). This osmotically-driven sympathoexcitatory response was significantly attenuated (~50%) by a previous bilateral microinjection of the V1a antagonist within the PVN (2 nmol in 100 nl, $P< 0.001$ *vs.* control, ***Fig.8C,D***). As shown in ***Fig.8E***, the intracarotid osmotic stimulation evoked a significant increase in VP release within the SON ($P< 0.001$, one way ANOVA repeated measures, n=7). These results indicate that osmotically-driven dendritic VP release participates in the recruitment of presympathetic neurons during a homeostatic challenge requiring an orchestrated neurosecretory and sympathetic response.

DISCUSSION

The two modalities by which the PVN commands the generation of complex homeostatic responses are represented in distinct neuronal populations, including neurosecretory neurons projecting to the median eminence or the posterior pituitary, and presympathetic neurons innervating the spinal cord and/or brainstem nuclei, including the rostroventrolateral medulla (RVLM) (Swanson and Sawchenko, 1980). Given its diverse, though well-characterized anatomical and functional organization, the PVN stands as an ideal brain region to study inter-population signaling modalities in the brain. Despite its highly integrative function, it is well-documented that neurosecretory and presympathetic PVN neuronal populations are anatomically compartmentalized, displaying minimal or complete lack of hard-wired interconnections (Hatton et al., 1985; Swanson and Kuypers, 1980; Swanson et al., 1980). This has led to the notion that polymodal homeostatic control by the PVN involves parallel processing of neuroendocrine and autonomic information. In this study, we challenged this prevailing idea by testing the novel hypothesis that dendritic release of peptides serves as an inter-population signal mediating crosstalk between neurosecretory and presympathetic PVN neuronal populations. Along with nigrostriatal dopaminergic neurons (Cheramy et al., 1981), hypothalamic MNNs are one the best-characterized prototypes of dendritic neurotransmitter release (Ludwig and Leng, 2006). Dendritic release of VP and OT from MNNs acts as powerful feedback signals by which MNNs auto-regulate their own activity, to optimize systemic hormone release in response to physiologically relevant challenges (Kombian et al., 1997; Ludwig and Leng, 1997). Results from the present study demonstrate that in addition to its autocrine actions, VP acts as a diffusible signal to bridge information across neurosecretory and presympathetic neuronal populations. This novel crosstalk involves Ca^{2+}-dependent dendritic release of VP, diffusion in the extracellular space, and activation of V1a VP receptors coupled to a CAN channel in presympathetic neurons. Lastly, we demonstrate this crosstalk modality to be critical for an optimal homeostatic sympathetic response to a central osmotic challenge (Bourque, 2008; Toney and Stocker, 2010).

Dendritically released VP mediates a neurosecretory-to-presympathetic neuronal crosstalk.

We found that selective activation of a single neurosecretory VP neuron (either by photolytic NMDA uncaging or direct current injection in dual-patch recordings) evoked a V1a receptor-mediated depolarization and firing discharge in neighboring presympathetic (PVN-RVLM) neurons. Several lines of evidence support that the underlying mechanism involved activation of a Ca^{2+}-activated non-selective cation (CAN) channel (Petersen, 2002), including: (a) VP induced in PVN-RVLM neurons an increase in $[Ca^{2+}]_I$ that preceded the enhanced membrane excitability; (b) intracellular Ca^{2+} dependency of the VP effect, (c) voltage-dependent properties of I_{VP}, including an outwardly rectifying I/V curve and (d) the I_{VP} reversal potential, characteristic of a mixed-cationic conductance. While our pharmacological (flufenamic acid), immunohistochemical and single-cell RTPCR experiments (***Fig.S2***) suggest the involvement of TRPM4 channels, recently reported to be present in MNNs (Teruyama et al., 2011), future studies are needed to identify the precise molecular identity of the underlying CAN channel.

Following bursts of action potentials, VP neurons express two types of opposing post-spike membrane potentials: AHPs and DAPs. These potentials temporally overlap, competing with each other to either inhibit or increase post-firing membrane excitability, respectively (Armstrong et al., 2010). We found that when prominent AHPs were observed in the stimulated VP neurons, the response latency of the presympathetic neurons was prolonged. This suggests that AHPs act as a “braking” system that efficiently regulate activity-dependent dendritic VP release, and consequently, the timing of the inter-neuronal crosstalk in the PVN.

MNNs project almost exclusively to the posterior pituitary (Swanson and Kuypers, 1980), with only a few reported cases of scarce axon collaterals, arising from, but terminating outside the PVN (Hatton et al., 1985). Thus, the topographical segregation between the dendritic and axonal terminal fields of MNNs minimized the possibility that photolytically-evoked VP released within the PVN originated from an axon terminal, rather than a dendritic source. This is further supported by our results showing that the evoked neurosecretory-presympathetic crosstalk persisted in the presence of TTX,

which prevents axonal but not somatodendritic release of neuropeptides from MNNs. Similar to dorsal raphe serotonin neurons (de Kock et al., 2006), NMDA was shown to evoke dendritic release from MNNs in the absence of action potentials (de Kock et al., 2004), and dendritic VP release involves a Ca^{2+}-dependent exocytotic event (Ludwig et al., 2002). Accordingly, we found that photolysis of caged-NMDA in the somata of VP neurons resulted in a rise in $[Ca^{2+}]_i$ both in neuronal somata and dendrites. This in turn was followed by an excitatory response in presympathetic neurons, which was prevented by a synaptic block media. Finally, intracellular Ca^{2+} chelation in VP neurons prevented the neurosecretory-presympathetic coupling observed in dual-patch recordings.

While the combined anatomical, imaging and electrophysiological data reported here strongly support a direct communication between neurosecretory and presympathetic neurons, we cannot conclusively rule out the participation of other intermediaries. For example, the evoked VP release from a single MNN could act in a recurrent positive feedback manner to recruit additional VP neurons to release further amounts of VP (Kombian et al., 1997; Ludwig and Leng, 1997). Moreover, dendritically released VP could also act on nearby astrocytes to evoke release of a potential gliotransmitters. However, our data showing that stimulation of VP neurons failed to consistently activate nearby astrocytes, and the fact that the neurosecretory-presympathetic coupling persisted following ablation of astrocyte function, would argue against this possibility.

Dendritically released VP acts as a diffusible inter-population signal contributing to homeostatic neurohumoral responses

Given its long half-life (~20 min in the brain (Mens et al., 1983)), VP is ideally suited to act as a diffusible signal, potentially affecting multiple neurons at relatively distant locations. We found the firing activity of presympathetic PVN neurons to be tonically stimulated by an endogenous VP “tone”, whose strength was enhanced either by increasing the activity of VP neurons, or by prolonging VP lifetime in the extracellular space (aminopeptidase block) (Chen and Pittman, 1999). Conversely, the strength of the VP tone was diminished when VP neuronal activity was inhibited (κ opiod agonist)(Brown et al., 1998), or when the coefficient of diffusion of molecules in the ECS

was lessened (5% dextran) (Piet et al., 2004). Thus, our findings support the ability of dendritically released VP from the neurosecretory population to act in a diffusible manner to modulate the activity of neighboring presympathetic neurons.

A central hyperosmotic challenge triggers a coordinated systemic release of VP, along with an increased renal sympathetic nerve activity (RSNA) (Bourque, 2008; Toney and Stocker, 2010). These responses are largely mediated by activation of neurosecretory and presympathetic SON/PVN neuronal populations, respectively (Antunes et al., 2006; Chen and Toney, 2001; Leng et al., 2001; Oliet and Bourque, 1993). In addition to systemic release, osmotic stimuli also evoke local dendritic release of VP (Leng and Ludwig, 2008), which serves as a "population feedback" signal by which VP neurons auto-regulate their own activity to optimize hormone secretion from their axonal terminals (Gouzenes et al., 1998). In this study, we found that a hyperosmotic-induced increase in RSNA was largely attenuated when V1a receptors within the PVN were locally blocked.

Given that VP MNNs are intrinsically osmosensitive (Oliet and Bourque, 1993), it is reasonable to speculate that osmotically-driven dendritic VP release effectively augmented the endogenous neurosecretory VP tone, directly stimulating in turn the neighboring presympathetic neuronal population. Alternatively, dendritically released VP could also act by increasing presympathetic neuronal responsiveness to forebrain glutamatergic afferent inputs, known to contribute to osmotically-driven sympathetic responses by the PVN (Antunes et al., 2006; Shi et al., 2007). This could occur either by strengthening osmosensitive glutamatergic afferents (i.e., pre- or post-synaptically), or simply by depolarizing the presympathetic resting membrane potential closer to spike threshold. We found that VP excitatory effects on presympathetic PVN neurons persisted in the presence of ionotropic glutamate receptor blockade, suggesting that a direct VP excitatory signal *per se* is sufficiently strong to evoke firing discharge and increase sympathetic outflow from the presympathetic neuronal population.

The extent to which other PVN neuronal populations are also targeted by dendritically released VP is at present unknown. Clearly, recruitment specificity is a critical factor for the generation of a physiologically relevant homeostatic responses,

which is likely achieved by the selective expression of V1a receptors in the relevant neuronal populations.

Collectively, our findings provide, to the best of our knowledge, the first demonstration that activity-dependent dendritic release of peptides constitutes an efficient inter-population signaling modality in the brain. More specifically, they support our hypothesis that a local crosstalk between hypothalamic neurosecretory and presympathetic neuronal populations plays an important role in the generation of central integrative homeostatic responses (Pittman et al., 1982). Finally, given that neurohumoral activation (a process involving elevated neurosecretory and sympathetic outflows) is a hallmark in prevalent diseases such as hypertension and heart failure (Cohn et al., 1984; Esler et al., 1995; Pliquett et al., 2004), our studies provide insights into potentially novel pathophysiological mechanism contributing to morbidity and mortality in these prevalent diseases.

EXPERIMENTAL PROCEDURES

Animals. Male Wistar rats (160-220 g) were purchased from Harlan laboratories (Indianapolis, IN), and housed in a 12 hr:12 hr light-dark cycle with access to food and water ad libitum. In a subset of experiments, we also used male heterozygous transgenic VP-eGFP Wistar rats (5-6 weeks old), in which VP neurons are endogenously fluorescent (Ueta et al., 2005). All procedures were carried out in agreement with the University of Georgia Health Sciences and the University of Nebraska Medical Center Institutional Animal Care and Use Committee guidelines, and were approved by the respective committees.

Retrograde tracing. To identify presympathetic RVLM-projecting PVN neurons (PVN-RVLM), rats were anesthetized (ketamine-xylazine mixture, 90 and 50 mg kg^{-1}, respectively, i.p.) and a stereotaxic apparatus was used to pressure inject 500 nl of rhodamine-labeled microspheres (Lumaflor, Naples, FL, USA) or cholera toxin B (CTB) (1%, List Biological Laboratories) into the RVLM (starting from Bregma: 12 mm caudal along the lamina, 2 mm medial lateral, and 8 mm ventral). Injection sites were contained within the caudal pole of the facial nucleus to ~ 1 mm more caudal, and were ventrally

located with respect to the nucleus ambiguous. The location of the tracer was verified histologically (Sonner et al., 2011). Injections located either more rostral or lateral to the targeted area did not result in PVN labeling, and these animals were discarded from the study. Animals were used 3-4 days after surgery.

Slice preparation. Rats were anesthetized with pentobarbital (50 mg kg^{-1}) and perfused through the heart with a cold sucrose solution (containing in mM: 200 sucrose, 2.5 KCl, 3 $MgSO_4$, 26 $NaHCO_3$, 1.25 NaH_2PO_4, 20 D-glucose, 0.4 ascorbic acid, 1 $CaCl_2$ and 2 pyruvic acid (290-310 mosmol l^{-1}). Rats were decapitated, brains dissected out, and coronal slices (200 μm) of the hypothalamus containing the PVN were cut in an oxygenated ice cold ACSF (containing in mM: 119 NaCl, 2.5 KCl, 1 $MgSO_4$, 26 $NaHCO_3$, 1.25 NaH_2PO_4, 20 D-glucose, 0.4 ascorbic acid, 2 $CaCl_2$ and 2 pyruvic acid; pH 7.4; 290-310 mosmol l^{-1}), using a vibroslicer (D.S.K. Microslicer, Ted Pella, Redding, CA). For synaptic blockade, a 0.2 mM $CaCl_2$ and 400 μM $CdCl_2$ ACSF was used. In other cases, a 0 mM $CaCl_2$ / 3 mM EGTA solution was used, as indicated. Slices were kept in a holding chamber containing ACSF (room temperature) until used.

Electrophysiology. Hypothalamic slices were transferred to a recording chamber and superfused with ACSF (30–32 °C) at a flow rate of ~3.0 ml min^{-1}. Conventional whole-cell patch clamp recordings were obtained as previously described (Sonner et al., 2011). Patch pipettes (4-7 MΩ) composed of thin walled (1.5 mm outer diameter, 1.17 mm inner diameter) borosilicate glass (GC150T-7.5, Clark, Reading, UK), were pulled on a horizontal electrode puller (P-97, Sutter Instruments, Novato, CA). The internal solution contained (mM): 135 potassium gluconate, 10 EGTA, 10 HEPES, 10 KCl, 0.9 MgATP, 0.3 NaGTP and 20 phosphocreatine (Na^+); pH 7.2-7.3. When noted, neurons were intracellularly labeled with Alexa Fluor 555 (100 μM) or biocytin (1%). Recordings were obtained with a Multiclamp 700A amplifier (Axon Instruments, Foster City, Ca) from fluorescently-labeled PVN-RVLM neurons located in the parvocellular ventromedial or dorsal cap subnuclei, or from eGFP-VP neurons, located in the lateral magnocellular subnucleus. Neurons were visualized with a combination of fluorescence illumination and infrared differential interference contrast (IR-DIC) videomicroscopy. The voltage-output was digitized at 16-bit resolution, 10 kHz (Digidata 1320A, Axon Instruments),

and saved on a computer for offline analysis. For current-clamp recordings, all protocols were run using an output gain of 5 and a Bessel filter of 2 kHz. Firing activity and membrane potential were recorded in continuous mode before and during application of drugs. For bath-applied drugs, mean values were calculated from a 2-min period before drug application, and in a 2-min period around the peak effect. For briefer applications (picospritzer) and uncaging, values were calculated from a 1-mi period before, and 10-20 sec period around the peak effect, using Clampfit (Axon Instruments, Foster City, Ca) or miniAnalysis (Synaptosoft Inc., NJ) software. DC current injection was used in an attempt to maintain neurons at a similar low level of basal firing activity, while holding them at an approximate membrane potential of -45 to -55 mV. The mean series resistance was monitored throughout the recording (< 20 MΩ) and data discarded if changes >20% were observed).

Confocal calcium imaging. Magnocellular neurosecretory neurons were loaded through the patch pipette with Fluo-5F pentapotassium salt (100 μM; Molecular Probes, Carlsbad, CA), as previously described(Filosa et al., 2006; Sonner et al., 2011). Once in the whole-cell mode, the dye was allowed to dialyze into the cell for at least 20 minutes before the initiation of the recordings, in order to allow complete dialysis of the dye. For astrocyte Ca^{2+} measurements, slices were incubated at room temperature (RT) in ACSF containing Rhod2-AM and pluronic acid (2.5 μg/ml). Imaging was conducted using the Yokogawa real time live cell laser confocal system combined with a highly-sensitive EMCCD camera (iXON+885, Andor Technology, South Windsor, CT). Fluorescence images were obtained using diode-pumped solid-state laser (Melles Griot, Carlsbad, CA) at 488 nm and emitted light at >495 (Fluo4) or 561 nm and emitted light >607 nm (Rhod2). Images were acquired at a rate of 4 Hz. The fractional fluorescence (F/F_0) was determined by dividing the fluorescence intensity (F) within a region of interest (ROI; 6 x 6 pixels ≈ 4.8 x 4.8 μm) by a baseline fluorescence value (F0) determined from 30 images before photolysis of caged-NMDA. Data was analyzed using Andor IQ software (Andor Technology).

Photolysis of caged-compounds. Uncaging was performed using the Andor Technology Revolution system (iXON EMCCD camera with the Yokogawa CSU 10,

confocal scanning unit). Slices were perfused with MNI-caged-NMDA (50 µM). A UV laser excitation (405 nm) was directed to a region of interest drawn on the image of identified PVN-RVLM or eGFP-VP somata through a 40x or 63x microscope objective. Based on the pixel dwell time (200-800 μs) and the ROI area scanned (~ 40 μm^2), the uncaging protocol lasted 180 – 720 ms. The confocality of the system allows for the photolysis beam to occur at the focal plane of choice, with minimal diffusion beyond the activated plane. Uncaging was done while simultaneously recording neuronal firing activity or $\Delta[Ca^{2+}]_I$ in the slice (see ***Figs.S4-S5***). For these experiments, an ACSF containing 20 μM Mg^{2+} was used to facilitate detection of evoked NMDA responses, although similar but smaller responses were also observed in control ACSF (*not shown*).

PVN microinjections and in vivo renal sympathetic nerve activity (RSNA) measurements. On the day of the experiment, rats were anesthetized with urethane (0.75g/kg i.p.) and α-chloralose (70mg/kg i.p.) and the left femoral artery was cannulated and connected to a computer-driven data recording and analyzing system (PowerLab, ADI instruments, Colorado springs, CO, USA) via a pressure transducer (Gould P23 1D) for recording arterial blood pressure and heart rate. The anesthetized rat was placed in a stereotaxic apparatus (Davis Kopf Instruments, Tujunga, CA, USA). A longitudinal incision was made on the head and the bregma was exposed. The coordinates for the PVN were determined from the Paxinos and Watson Atlas. They were 1.5mm posterior to the bregma, 0.4mm lateral to the midline, and 7.8mm ventral to the dura. A small burr hole was made in the skull. For the microinjections, a thin needle (0.5mm OD and 0.1mm ID) connected to a micro syringe (0.5ml; model 7000.5 Hamilton micro syringe) was lowered into the PVN. To record RSNA, the left kidney was exposed through a retroperitoneal flank incision. A branch of the renal nerve was isolated from the fat and connective tissue and was placed on a pair of thin bipolar platinum electrodes. The nerve-electrode junction was insulated electrically from the surrounding tissue with a silicone gel (Wacker Sil-Gel, 604 A B). The electrical signal was amplified (10000 times) with a Grass amplifier (P55) with a high- and low-frequency cutoff of 1000 and 100Hz, respectively. The output signal from the Grass amplifier was directed to a computer-run data acquisition system (PowerLab, ADI instruments,

Colorado springs, CO, USA) to record and integrate the raw nerve discharge. The signal recorded at the end of the experiment (after the rat was dead) was deemed as background noise. The basal value of the nerve activity was defined by subtracting the background noise from the actual nerve activity value before the administration of drugs into the PVN. The peak response of RSNA to the administration of drugs into the PVN during the experiment (averaged over a period of 20-30s) was subsequently expressed as a percent change from baseline (Biancardi et al., 2011).

Central hyperosmotic stimulation and VP microdialysis. Central hyperosmotic stimulation was achieved by delivering graded concentrations of NaCl (0.3, 0.9, and 2.1 osmol/l) through an internal carotid artery (ICA) catheter. The ICA is the main artery supplying limbic areas, including the hypothalamus, and this approach was previously shown to elicit efficiently and reproducibly central, but not peripheral hyperosmolarity (Chen and Toney, 2001). Injections were delivered in a volume of 300 μl over a period of 10-15 seconds. For microdialysis, rats were anaesthetized with urethane (ethyl carbamate, intraperitoneally 1.2 g/kg, Sigma Chemical Co., UK). In-house designed microdialysis probes (molecular weight cut-off of 6 kDa, Fleaker® Hollow Fibre, Spectrum® Med. Inc., USA) were stereotaxically implanted with the U-shaped tip located within or adjacent to the right SON (1.0 mm posterior to bregma; 1.7 mm lateral to midline; 9.3 mm below the surface of the skull, as previously described (Ludwig et al., 2002). After an equilibration period of at least 1 h, consecutive 30-min dialysis samples were collected at a flow rate of 3 μl/min. After two 30-min baseline periods, rats were stimulated osmotically as described above, and a further two consecutive dialysate samples were collected, frozen and stored at -20^{o}C until assay for vasopressin. The vasopressin content in the microdialysates was measured by a highly sensitive and selective radioimmunoassay (detection limit: 0.1 pg/sample; cross-reactivity less than 0.7%) as previously described (Landgraf et al., 1995).

Immunohistochemistry. Rats were anesthetized with pentobarbital (50 mg kg^{-1}) and perfused transcardially in 4% paraformaldehyde in 0.01 M phosphate buffer saline (PBS). Brains were then removed, postfixed for 2-4 hours, cryoprotected in 30%

sucrose in 0.01 M PBS (4 °C, 3 days), and then stored at -80 °C until further use. Coronal slices (30 µm) containing the PVN were cut and collected in 0.01 M PBS. Slices were then incubated in 0.01 M PBS with 0.1% Triton X-100, 0.04% NaN_3 ($PBS_{TX}NaN_3$), and 5% normal horse serum for 1 hour at room temperature. Slices were then rinsed thoroughly with 0.01 M PBS, followed by incubation with one or a combination of the following primary antibodies rabbit (1:100; Millipore) or goat (1:50; Santa Cruz) anti-V1a receptor; goat anti-CTB (1:2500; List Biological Laboratories); rabbit anti-TRPM4 (1:2000, kindly donated by Dr. Teruyama, LHSU, Baton Rouge); rabbit anti-microtubule-associated protein 2 (MAP2, 1:500, Sigma); Mouse anti-dopamine β hydroxylase (DBH, 1:20,000, Millipore). Incubation in primary antibodies (overnight at 4 °C in $PBS_{TX}NaN_3$) where followed by specific fluorescently labeled secondary antibodies (1:250; Jackson ImmunoResearch Laboratories, West Grove, Pennsylvania, USA) for 4 hours at 4 °C in $PBS_{TX}NaN_3$. Slices were then rinsed thoroughly, mounted, and visualized using confocal microscopy (Carl Zeiss MicroImaging, Inc., Thornwood, NY, USA; 63x oil immersion, zoomed x2; single optical plane = 0.5 µm thick) (Biancardi et al., 2010). Negative controls included incubations in the absence of primary antibodies and preabsorption with the respective antigen peptide, as previously done (Biancardi et al., 2010). Both of these control approaches resulted in absence of staining (see for example ***Fig.S1***).

Single cell RTPCR. Single cell RT-PCR was carried out as previously described with minor modification (Sonner et al., 2011). The cytoplasm of the patched neuron, taking care not to contain the nucleus, was pulled into a patch pipette containing 2 µl DEPC-treated water, and then mixed with 1 µl of RNase inhibitor (Applied Biosystems, Foster city, CA, USA) and immediately frozen in liquid nitrogen, and kept at -80 C until processed. RT for cDNA was carried out with iScript cDNA Synthesis Kit (BIO-RAD, CA, USA) according to manufacturer's manual. PCR amplification was performed with a fraction of cDNA as a template. The mixture of PCR reaction contained (in µl): 1 of 10µM each primer, 10 of 2× master mix buffer (Go Taq Green Master Mix, Promega), and 8 of the cDNA template. The annealing temperature in the thermal cycler was 60 °C and 50 cycles were performed. A nested approach was used to quantify V1a receptor

mRNA. The primers used included: First nested PCR: 5′-cgaggtgaacaatggcactaaaac-3′ and 5′-tgtgatggaagggttttctgaatc-3′; Second nested PCR 5′-tcatctgctaccacatctggcg-3′ and 5′-gtgtaaccaaaagccccttatgaaag-3′; Primers for TRPM4: 5′-cctgcaggcccaggtagaga-3′ and 5′-ttcagcagagcgtccatgag-3′. GAPDH primers: 5'-ttcaacggcacagtcaagg-3' and 5'-tggttcacacccatcacaaa-3'. All primers were synthesized by Intergrated DNA technologies (Iowa, USA). Final PCR products were electrophoresed on a 2% agarose gels in TAE buffer (40mM Tris-acetate, 1mM EDTA, pH 8) containing 0.5 µg/ml ethidium bromide, observed UV light, and photographed. Negative controls were performed by replacing cDNA with water.

Statistical Analysis. All values are expressed as means ± S.E.M. In most cases, unpaired or paired t tests were used, as indicated. One or two-way ANOVA tests with Bonferroni posthoc tests were used as needed. Pearson's correlation test was used to determine if correlations existed between two parameters. Differences were considered significant at $P < 0.05$. All statistical analyses were conducted using GraphPad Prism (GraphPad Software, San Diego, CA).

Drugs. All drugs with the exception of MNI-caged-NMDA (Tocris, Ellisville, MO USA), were purchased from Sigma-Aldrich (St. Louis, MO, USA). For simplicity, the selective V1a antagonist β-Mercapto-β,β-cyclopentamethylenepropionyl[1], O-me-Tyr[2], Arg[8]-Vasopressin (Sigma V2255), is referred to as "V1a antagonist" throughout the manuscript.

FIGURE LEGENDS

Figure 1. Dendro-somatic and dendro-dendritic interrelationships between presympathetic and magnocellular neurosecretory PVN neurons. (**A**) Confocal image showing the topographical segregation between immunoreactive magnocellular neurosecretory vasopressin (VP, green) and retrogradely-labeled presympathetic PVN-RVLM (red) neuronal somata. In (**B**) and (**C**), the squared regions are shown at progressively higher magnification, to better depict the presence of thick and varicose VP dendrites within the presympathetic neuronal compartment. Additional examples of VP dendrites extending from the lateral magnocellular subnucleus into the three main presympathetic PVN subnuclei, including the dorsal cap (**D**), parvocellular ventromedial (**E**) and parvocelluar posterior (**F**) are shown. (**G**) PVN-RVLM neurons surrounded by VP dendrites are shown at high magnification. (**H**) Low magnification image of the PVN showing that the vast majority of immunoreactive vasopressin (green) and oxytocin (red) axons emerge from the PVN, running laterally and ventrally towards the median eminence. **(I**) Image showing thick, immunoreactive VP processes (green), which are also MAP2 immunoreactive (white, arrows) nearby a PVN-RVLM neuron (red, asterisk). Note the abundance of MAP2 processes that are negative for VP. (**J**) Image showing DBH immunoreactive boutons (white, arrows) abutting VP-immunoreactive processes (green) near a PVN-RVLM neuron (red, asterisk). Vertical and horizontal arrows point dorsally and ventrally, respectively. 3V: third ventricle. Scale bars in A-G= 20 μm; H= 200 μm; I, J= 5 μm.

Figure 2. Presympathetic PVN neurons express functional V1a receptors. (**A**) Sample confocal image at low magnification showing CTB-retrogradely-labeled PVN-RVLM neurons (blue), and V1a receptor immunoreactivity (green, Millipore primary antibody) in the PVN. In (**B**) and (**C**), examples of two PVN-RVLM neurons showing dense V1a immunoreactive clusters, respectively, are depicted. In (**D**), the squared area in (**B**) is shown at an expanded scale, to better show V1a immunoreactive clusters (arrows) located at the surface of the shown dendrite. (**E**) Single-cell V1a mRNA expression in identified PVN-RVLM and eGFP-VP neurons. A non-template negative

control is shown in the right lane, and a small piece of a DNA ladder is shown in the left lane. (**F**) A puff of VP (1 μM, arrowheads) delivered directly onto a presympathetic PVN-RVLM neuron evokes a high-frequency burst of action potentials. (**G**) Sample trace showing that in the presence of tetrodotoxin (TTX 0.5 μM), puffs of VP of decremental durations depolarized a presympathetic PVN neuron in a proportionally decremental manner. Note the presence of Ca^{2+} spikes (arrow). (**H**) Summary data of VP effects on firing activity and (**I**) membrane potential in presympathetic neurons (n=16). Scale bars in A, B= 20 μm; D= 2.5 μm.

Figure 3. VP effects on presympathetic neurons involves an increase in $[Ca^{2+}]_I$ and activation of a CAN channel. (**A**), Sample traces showing simultaneous $\Delta[Ca^{2+}]_I$ (lower) and membrane potential (upper) measurements in a PVN-RVLM neuron in response to bath-applied VP (1 μM, line). Note that the increase in $\Delta[Ca^{2+}]_I$ preceded the increase in firing discharge. (**B**), Representative pseudocolor (upper) and black and white (lower) images of VP-evoked Ca^{2+} changes in the PVN-RVLM neuron shown in A. Image numbers correspond to the time points shown in A. (**C**), Summary data showing mean VP-evoked Ca^{2+} changes (F/F_0) in presympathetic PVN neurons (n=8). (**D**), Sample trace and summary data showing that chelation of intracellular Ca^{2+} with BAPTA (10 mM) in the patch pipette prevented VP excitatory effect (puff, arrowhead) in presympathetic PVN neurons (n=8). (**E**) Sample trace in voltage-clamp mode showing a VP-mediated (puff, arrowhead) inward current (I_{VP}) in a presympathetic PVN neuron. The right panel shows a mean I/V plot of I_{VP} evoked at various holding potentials (n=5). **P< 0.01.

Figure 4. Photo-activation of neurosecretory VP neurons evokes a V1a receptor-mediated excitatory response in neighboring presympathetic neurons. (A1) Inward currents evoked in a patched eGFP-VP neuron following photolysis of caged-NMDA onto various somatodendritic regions of interest (ROI) (1-3). Note that photolysis in an ROI a few microns away from the recorded neuron (4) failed to evoke a response. (**A2**), Repetitive laser photolysis of caged NMDA onto the same eGFP-VP neuron evoked reproducible inward currents (upper trace), membrane depolarizations (lower

trace), and bursts of action potentials (right traces). (**B1**) Slice containing a patched presympathetic PVN-RVLM neuron (red, asterisk) and neighboring eGFP-VP neurons (green, 1-4) that were activated with photolysis of caged-NMDA. (**B2**) Direct uncaging of NMDA onto the patched presympathetic neuron (asterisk, yellow flashes) evoked a burst of action potentials. (**B3**) Burst of action potentials recorded in the patched presympathetic neuron in response to uncaging of NMDA onto the eGFP-VP neurons shown in **B1 (**1-4, red flashes). Note the delayed response in the PVN-RVLM neurons compared to B2. (**C1**) Combined DIC and fluorescence image of a slice containing a patched presympathetic neuron (asterisk) and neighboring eGFP-VP neurons (green). (**C2**) Presympathetic neuronal responses to uncaging of NMDA onto the recorded PVN-RVLM neuron neuron (upper traces) or onto an eGFP-VP neuron (arrow in **C1**, and lower traces), in control ACSF (left) and in the presence of a V1a receptor antagonist (right). (**C3**) Summary data of mean changes in the number of action potentials, action potential frequency, and membrane potential in presympathetic PVN-RVLM neurons, evoked by photolysis of caged-NMDA onto the presympathetic neurons themselves (n=11, left) or onto eGFP-VP neurons in the absence (n=38, middle) or presence (n=7, right) of the V1a antagonist. *P< 0.01 and **P< 0.001 vs. respective ACSF.

Figure 5. The NMDA-mediated crosstalk between neurosecretory VP and presympathetic PVN-RVLM neurons is not dependent on action potential firing. (**A1**) Sample of a slice containing a patched presympathetic PVN-RVLM neuron that was loaded with alexa fluor 555 (red, asterisk) and neighboring eGFP-VP neurons (green) that were photoactivated with caged-NMDA. (**A2**) Representative traces obtained from the recorded PVN-RVLM neuron following 5 repetitive photolysis of caged-NMDA directly onto the recorded cell (upper trace, yellow flashes), or in response to simultaneous photolysis onto the three eGFP-VP neurons (1-3, red flashes) shown in A1, in control ACSF + 1 μM TTX (middle trace), and following bath application of the V1a receptor antagonist + TTX (lower trace). (**B**) Summary data of mean changes in PVN-RVLM membrane potential evoked in the presence of TTX following photolysis of caged-NMDA onto the presympathetic neurons themselves (n=6, blue bar), or onto eGFP-VP neurons (red bars) in the absence (n=18, middle bar) or presence (n=14, right

bar) of the V1a receptor antagonist. (**C1**) Another example showing a recorded presympathetic PVN-RVLM neuron (alexa fluor 555, red) and a photoactivated eGFP-VP neuron (green, arrow). (**C2**) Sample traces obtained from the PVN-RVLM neuron from C1, following photolysis of caged-NMDA in the presence of 1 μM TTX directly onto the PVN-RVLM neuron itself (asterisk, upper trace, yellow flash), or onto an eGFP-VP neuron (red flashes), in control ACSF (middle trace) and following bath application of the V1a receptor antagonist (lower trace), in the presence of TTX. *P< 0.01 vs. respective ACSF. Scale bars: 15 μm.

Figure 6. Neurosecretory-presympathetic crosstalk unveiled during dual-patch recordings from eGFP-VP and PVN-RVLM neurons. (**A1**) Sample pair of intracellularly labeled (Alexa 633, blue, arrows) PVN neurons during simultaneous dual-patch recordings. The identity of the patched neurons as eGFP-VP (cyan, single arrow) and retrogradely-labeled PVN-RVLM (purple, double arrow) is shown in **A2**. **(B1)** Electrically evoked bursting activity in the eGFP-VP neuron resulted in a delayed membrane depolarization and increased firing discharge in the neighboring PVN-RVLM neuron. Note the pronounced AHP following action potential firing in the eGFP-VP neuron (filled arrowhead). **(B2)** Another sample of paired recordings showing a similar response. Note however the lack of AHP in the eGFP-VP neuron (empty arrowhead), and the shorter latency of the evoked PVN-RVLM response. **(C)** Sample of a paired recording in which the eGFP-VP neuron was dialysed with BAPTA. Note the lack of response in the PVN-RVLM neuron. **(D)** Sample of a paired recording in the presence of L-aminoadipic acid (L-AAA, 250 μM, 30 min), showing an increase in PVN-RVLM firing activity following stimulation of the eGFP-VP neuron. Note the presence of a DAP in the eGFP-VP neuron (double filled arrowheads), and the brief latency for the evoked PVN-RVLM response. (**E**) Comparison of the mean inter-neuronal coupling latency in eGFP-VP neurons displaying or not an AHP following the evoked burst of action potentials (n=10 and 8, respectively). (**F**) Summary data of mean changes in PVN-RVLM membrane potential (left) and firing activity (right) following direct stimulation of eGFP-VP neurons in control ACSF (n=13), V1a antagonist (n=7), intracellular BAPTA in the stimulated eGFP-VP neuron (n=5) and in the presence of L-AAA (n=5). **G1-G3**, Another

representative example of dual-patched and intracellularly-labeled eGFP and PVN-RVLM neurons. (**G1)**, Single focal plane of a confocal image showing eGFP-VP (green) and PVN-RVLM (red) neurons. The recorded PVN-RVLM neuron was intracellularly filled with Alexa 633 (arrow, colocalization= purple), and the recorded eGFP-VP neuron was intracellularly filled with Alexa 555 (arrowhead, colocalization= yellow). In **G2**, the same image as in A1, but a confocal stack of 10 images is shown to better depict the dendritic processes of the recorded neurons. The blue color has been transformed to white for better clarity. Asterisk points to a dendritic end of the eGFP-VP (Alexa 555 filled) neuron. In **G3,** the squared area in G2 is shown at a magnified scale. **P< 0.001 vs. AHP; $^{+}$P< 0.05 and $^{\#}$P< 0.01 vs. V1a antagonist and BAPTA, respectively. Scale bars: A, B= 25 μm; G1, G2= 20 μm; G3= 10 μm. Action potentials were cropped.

Figure 7. An activity-dependent diffusible pool of dendritically-released VP tonically modulates presympathetic neuronal activity. (**A**) Sample trace showing a hyperpolarization and diminished firing discharge of a presympathetic neuron following bath application of the V1a receptor blocker (1 μM). At the arrow, DC current injection was applied to bring the membrane potential back to control levels, to show that the V1a antagonist efficiently blocked the neuronal response to a VP puff (1 μM, arrowhead). (**B**) Summary data of the effects of the V1a receptor antagonist on firing frequency and membrane potential of presympathetic neurons (n=14). (**C**) Sample trace showing a blunted effect of the V1a receptor antagonist in the presence of the κ receptor agonist U-50488 (1 μM). (**D**) Summary data of the effects of the V1a antagonist on presympathetc neuronal firing in control ACSF (K^+ 2.5 mM), high K^+ ACSF (8.5 mM) and in U-50488 (K^+ 2.5 mM) (n= 6, 7 and 8, respectively). (**E**) Sample traces and summary data showing the effects of the aminopeptidase blocker amastatin (10 μM, 10 min) in control ACSF and in the presence of the V1a receptor antagonist (n=8 in each group). *P< 0.05; **P< 0.01 and ***P< 0.001.

Figure 8. Dendritic release of VP within the PVN contributes to sympathoexcitatory homeostatic responses following a central hyperosmotic challenge. (**A**) Representative traces showing changes in raw (lower) and integrated

(upper) renal sympathetic nerve activity (RSNA) following administration of VP (16 pmol) onto the PVN. (**B**) Summary data showing dose-dependent increases in RSNA after microinjections of VP (8, 16 and 32 pmol) onto the PVN ($P< 0.02$, one way ANOVA, n=9). (**C**) Representative traces showing changes in RSNA following intra-carotid infusions of an isosmotic (NaCl 0.3 osmol/l) or hyperosmotic (NaCl 2.1 osmol/l) solution, following bilateral microinjections of ACSF or of the V1a receptor antagonist ((2 nmol/100 nl, 6-10 mins before the osmotic challenge) onto the PVN. Note the increase in RSNA evoked by the hyperosmotic challenge in control ACSF (arrow) but not in the presence of the V1a receptor antagonist. (**D**) Summary data showing dose-dependent increases in RSNA after intra-carotid infusions of NaCl (0.3, 0.9 and 2.1 osmol/l) in animals that received an intra-PVN microinjection of either ACSF or the V1a receptor antagonist (*$P< 0.0001$ *vs.* respective ACSF, n=7). (**E**) Summary data showing increased VP content in 30-min microdialysates sampled from the SON before and after an intracarotid infusion of NaCl 2.1 osmol/l (arrow) (*$P< 0.05$ *vs.* basal levels, n=7).

SUPPLEMENTARY FIGURE LEGENDS

Figure S1. V1a receptor immunoreactivity in presympathetic PVN neurons. Sample confocal images showing V1a receptor immunoreactivity (***A1, B1, C1,*** green Santa Cruz primary antibody) and retrogradely-labeled PVN-RVLM neurons (***A2, B2, C2***, red, asterisks). In ***A3***, ***B3***, and ***C3***, images were superimposed. Arrows point to V1a immunoreactive clusters at the surface of the PVN-RVLM neurons. The *insets* in ***A3*** and ***B3*** show a portion of the PVN-RVLM neurons (rectangles) at expanded scales. Within the *insets*, arrows and arrowheads point to V1a cluster possibly located near the neuronal surface membrane and/or at presynaptic terminals, respectively. Images in ***C*** were obtained from tissue in which the antibody was preabsorbed with the corresponding antigen (5-fold molar excess relative to IgG concentration). Scale bars: A3-C3: 10 μm; inset in B3: 2.5 μm.

Figure S2. Expression of functional TRPM4 channels in presympathetic PVN neurons. (**A**) Sample confocal image at low magnification showing TRPM4 (green), and retrogradely-labeled PVN-RVLM neurons (red). The asterisk indicates the center of the lateral magnocellular subnucleus. (**B, C, D**) Three different samples at higher magnification showing TRMP4 immunoreactive (left, green) PVN-RVLM neurons (right, red). (**E**) Single-cell TRMP4 mRNA expression in identified PVN-RVLM neurons. A non-template negative is shown in the right lane, and a small piece of a DNA ladder is shown in the left lane. (**F**) Sample traces showing VP effects (puff, arrowheads) on a presympathetic PVN neuronal firing activity before (left) and after (right) bath application of flufenamic acid (FFA, 200 μM), a relative selective blocker of TRPM4/5 channels. The right graph shows the summary data (n=9). ***P< 0.001. Scale bars in A= 50 μm; B, C, D= 10 μm. 3V= third ventricle.

Figure S3. Identification of presympathetic and neurosecretory VP neurons using retrograde tract tracing in eGFP-AVP transgenic rats. (**A**) Sample confocal image of a PVN slice showing large eGFP-VP neurons (green) in the lateral magnocellular subnucleus (LM), along with smaller retrogradely-labeled PVN-RVLM neurons (red) in the dorsal cap (DC) and parvocellular ventromedial (PaV) subnculei. The inset shows

dense eGFP staining in the posterior pituitary (PP) of an eGFP-VP rat. (**B**) Confocal micrograph showing high degree of colocalization (yellow) between eGFP (green) and vasopressin (red) immunoreactivity in the PVN. (**C**) Confocal micrograph showing lack of colocalization between eGFP (green) and oxytocin (red) immunoreactivity in the PVN. Scale bars: (A)= 40 μm; *inset*: 400 μm (B) and (C)= 15 μm. 3V: third ventricle. Vertical and horizontal arrows point dorsally and medially, respectively.

Figure S4. Changes in somatodendritc $[Ca^{2+}]_i$ levels in eGFP-VP neurons in response to laser photolysis of caged-NMDA. (**A**) Sample showing that photolysis of caged-NMDA onto the soma of a patched eGFP-VP neuron evoked a rapid and transient change in dendritic $[Ca^{2+}]_i$ (red arrows). Image 1 is a projection image of the recorded neuron through a Z stack (40 μm). Single confocal planes before, during, and after (4 s) photolysis of caged-NMDA are shown in images 2-4, respectively. (**B**) Plots of changes in dendritic $[Ca^{2+}]_i$ (F/F0) as a function of time (obtained from the ROI show in **A1**), following NMDA uncaging in the soma of the eGFP-VP neuron using increasing laser pixel dwelling times. Traces were purposely shifted in the X-axis for their better comparison. (**C**) Summary data showing that changes in dendritic $[Ca^{2+}]_i$ following somatic uncaging of NMDA was dependent on the laser pixel dwelling time ($F= 4.3$, $P< 0.01$, 1 way ANOVA, n=6). *$P< 0.05$ *vs.* 100 and 200 μs dwell times). Scale bar in **A** = 15 μm.

Figure S5. Blockade of NMDA receptors in presympathetic PVN-RVLM neurons does not prevent the excitatory effect mediated by photolysis of caged-NMDA onto eGFP-VP neurons. (**A**) Sample of a combined DIC and fluorescence image of a slice containing a patched presympathetic PVN-RVLM neuron that was dialysed with the NMDA receptor blocker MK801 (1 mM, asterisk), and a neighboring eGFP-VP neuron (green, 1). (**B**) Lack of response to direct photolysis of caged-NMDA onto the patched PVN-RVLM neuron (upper trace, yellow flash). The middle and lower traces show the response of the same PVN-RVLM neuron to photolysis of caged-NMDA onto the eGFP-VP neuron (1, red flashes) in control ACSF and following bath application of the V1a receptor antagonist, respectively.

Figure S6. Photolysis of caged-NMDA onto eGFP-VP neurons failed to evoke increases in intracellular Ca^{2+} in the majority of nearby astrocytes. (**A**) Sample of Rhod-2 labeled astrocytes (red, 1-5) in the vicinity of an eGPF-VP neuron (green, arrow) photoactivated with caged-NMDA. (**B**) Traces showing ΔCa^{2+} levels (F/F0) in the respective astrocytes shown in A1, following NMDA uncaging onto the eGFP-VP neuron (arrow and vertical line). Note the delay increase in ΔCa^{2+} (asterisks) in astrocytes 1-3. (**C**) Summary data showing the total number of negative and positive responding astrocytes following NMDA uncaging onto 33 different eGFP-VP neurons. Scale bar in A1= 15 μm.

Figure S7. Activation of κ opioid receptors robustly inhibits firing discharge in identified eGFP-VP neurons. (**A**) Sample trace showing a robust membrane hyperpolarization and inhibition of firing activity of an eGFP-VP neuron evoked by bath application of the κ receptor agonist U-50488 (1 μM). The summary data (n= 5) is shown in (**B**). (**C**) Sample trace obtained from a presympathetic PVN-RVLM neuron in the presence of the V1a receptor antagonist, showing lack of effect of U-50488 (1 μM) on firing activity. The summary data (n= 4) is shown in (**D**). **P< 0.01.

ACKNOWLEDGMENTS

We would like to thank Professor Rainer Landgraf (Munich, Germany) for analyzing the microdialysis samples, Dr. Ryoichi Teruyama (Baton Rouge, USA), for the kind donation of the TRPM4 antibody; and Professor Gareth Leng (Edinburgh, UK) for critical reading of the manuscript. This work was supported by NIH R01-HL090948-01 (JES) and BBSRC BB/J004723/1 (ML).

REFERENCES

Antunes, V.R., Yao, S.T., Pickering, A.E., Murphy, D., and Paton, J.F. (2006). A spinal vasopressinergic mechanism mediates hyperosmolality-induced sympathoexcitation. J Physiol *576*, 569-583.

Armstrong, W.E., Wang, L., Li, C., and Teruyama, R. (2010). Performance, properties and plasticity of identified oxytocin and vasopressin neurones in vitro. J Neuroendocrinol *22*, 330-342.

Biancardi, V.C., Campos, R.R., and Stern, J.E. (2010). Altered balance of gamma-aminobutyric acidergic and glutamatergic afferent inputs in rostral ventrolateral medulla-projecting neurons in the paraventricular nucleus of the hypothalamus of renovascular hypertensive rats. J Comp Neurol *518*, 567-585.

Biancardi, V.C., Son, S.J., Sonner, P.M., Zheng, H., Patel, K.P., and Stern, J.E. (2011). Contribution of central nervous system endothelial nitric oxide synthase to neurohumoral activation in heart failure rats. Hypertension *58*, 454-463.

Bourque, C.W. (2008). Central mechanisms of osmosensation and systemic osmoregulation. Nat Rev Neurosci *9*, 519-531.

Brown, C.H., Ludwig, M., and Leng, G. (1998). kappa-opioid regulation of neuronal activity in the rat supraoptic nucleus in vivo. J Neurosci *18*, 9480-9488.

Buijs, R.M., and Van Eden, C.G. (2000). The integration of stress by the hypothalamus, amygdala and prefrontal cortex: balance between the autonomic nervous system and the neuroendocrine system. Prog Brain Res *126*, 117-132.

Chen, Q.H., and Toney, G.M. (2001). AT(1)-receptor blockade in the hypothalamic PVN reduces central hyperosmolality-induced renal sympathoexcitation. Am J Physiol Regul Integr Comp Physiol *281*, R1844-1853.

Chen, X., and Pittman, Q.J. (1999). Vasopressin and amastatin induce V(1)-receptor-mediated suppression of excitatory transmission in the rat parabrachial nucleus. J Neurophysiol *82*, 1689-1696.

Cheramy, A., Leviel, V., and Glowinski, J. (1981). Dendritic release of dopamine in the substantia nigra. Nature *289*, 537-542.

Cohn, J.N., Levine, T.B., Olivari, M.T., Garberg, V., Lura, D., Francis, G.S., Simon, A.B., and Rector, T. (1984). Plasma norepinephrine as a guide to prognosis in patients with chronic congestive heart failure. N Engl J Med *311*, 819-823.

de Kock, C.P., Burnashev, N., Lodder, J.C., Mansvelder, H.D., and Brussaard, A.B. (2004). NMDA receptors induce somatodendritic secretion in hypothalamic neurones of lactating female rats. J Physiol *561*, 53-64.

de Kock, C.P., Cornelisse, L.N., Burnashev, N., Lodder, J.C., Timmerman, A.J., Couey, J.J., Mansvelder, H.D., and Brussaard, A.B. (2006). NMDA receptors trigger neurosecretion of 5-HT within dorsal raphe nucleus of the rat in the absence of action potential firing. J Physiol *577*, 891-905.

Ely, D.L. (1995). Organization of cardiovascular and neurohumoral responses to stress. Implications for health and disease. Ann N Y Acad Sci *771*, 594-608.

Esler, M.D., Lambert, G.W., Ferrier, C., Kaye, D.M., Wallin, B.G., Kalff, V., Kelly, M.J., and Jennings, G.L. (1995). Central nervous system noradrenergic control of sympathetic outflow in normotensive and hypertensive humans. Clin Exp Hypertens *17*, 409-423.

Filosa, J.A., Bonev, A.D., Straub, S.V., Meredith, A.L., Wilkerson, M.K., Aldrich, R.W., and Nelson, M.T. (2006). Local potassium signaling couples neuronal activity to vasodilation in the brain. Nat Neurosci *9*, 1397-1403.

Fuxe, K., Dahlstrom, A., Hoistad, M., Marcellino, D., Jansson, A., Rivera, A., Diaz-Cabiale, Z., Jacobsen, K., Tinner-Staines, B., Hagman, B.*, et al.* (2007). From the Golgi-Cajal mapping to the transmitter-based characterization of the neuronal networks leading to two modes of brain communication: wiring and volume transmission. Brain Res Rev *55*, 17-54.

Galarreta, M., and Hestrin, S. (2001). Spike transmission and synchrony detection in networks of GABAergic interneurons. Science *292*, 2295-2299.

Ghamari-Langroudi, M., and Bourque, C.W. (2002). Flufenamic acid blocks depolarizing afterpotentials and phasic firing in rat supraoptic neurones. J Physiol *545*, 537-542.

Gouzenes, L., Desarmenien, M.G., Hussy, N., Richard, P., and Moos, F.C. (1998). Vasopressin regularizes the phasic firing pattern of rat hypothalamic magnocellular vasopressin neurons. J Neurosci *18*, 1879-1885.

Guan, J.L., Kageyama, H., Wang, Q.P., Takenoya, F., Kita, T., Matsumoto, H., Ohtaki, T., and Shioda, S. (2005). Electron microscopy examination of galanin-like peptide (GALP)-containing neurons in the rat hypothalamus. Regul Pept *126*, 73-78.

Hatton, G.I., Cobbett, P., and Salm, A.K. (1985). Extranuclear axon collaterals of paraventricular neurons in the rat hypothalamus: intracellular staining, immunocytochemistry and electrophysiology. Brain Res Bull *14*, 123-132.

Kombian, S.B., Mouginot, D., and Pittman, Q.J. (1997). Dendritically released peptides act as retrograde modulators of afferent excitation in the supraoptic nucleus in vitro. Neuron *19*, 903-912.

Landgraf, R., Neumann, I., Holsboer, F., and Pittman, Q.J. (1995). Interleukin-1 beta stimulates both central and peripheral release of vasopressin and oxytocin in the rat. Eur J Neurosci *7*, 592-598.

Landgraf, R., and Neumann, I.D. (2004). Vasopressin and oxytocin release within the brain: a dynamic concept of multiple and variable modes of neuropeptide communication. Front Neuroendocrinol *25*, 150-176.

Leng, G., Brown, C.H., Bull, P.M., Brown, D., Scullion, S., Currie, J., Blackburn-Munro, R.E., Feng, J., Onaka, T., Verbalis, J.G.*, et al.* (2001). Responses of magnocellular neurons to osmotic stimulation involves coactivation of excitatory and inhibitory input: an experimental and theoretical analysis. J Neurosci *21*, 6967-6977.

Leng, G., and Ludwig, M. (2008). Neurotransmitters and peptides: whispered secrets and public announcements. J Physiol *586*, 5625-5632.

Ludwig, M. (1998). Dendritic release of vasopressin and oxytocin. J Neuroendocrinol *10*, 881-895.

Ludwig, M., and Leng, G. (1997). Autoinhibition of supraoptic nucleus vasopressin neurons in vivo: a combined retrodialysis/electrophysiological study in rats. Eur J Neurosci *9*, 2532-2540.

Ludwig, M., and Leng, G. (2006). Dendritic peptide release and peptide-dependent behaviours. Nat Rev Neurosci *7*, 126-136.

Ludwig, M., Sabatier, N., Bull, P.M., Landgraf, R., Dayanithi, G., and Leng, G. (2002). Intracellular calcium stores regulate activity-dependent neuropeptide release from dendrites. Nature *418*, 85-89.

McBean, G.J. (1994). Inhibition of the glutamate transporter and glial enzymes in rat striatum by the gliotoxin, alpha aminoadipate. Br J Pharmacol *113*, 536-540.
Mens, W.B., Witter, A., and van Wimersma Greidanus, T.B. (1983). Penetration of neurohypophyseal hormones from plasma into cerebrospinal fluid (CSF): half-times of disappearance of these neuropeptides from CSF. Brain Res *262*, 143-149.
Min, M.Y., Rusakov, D.A., and Kullmann, D.M. (1998). Activation of AMPA, kainate, and metabotropic receptors at hippocampal mossy fiber synapses: role of glutamate diffusion. Neuron *21*, 561-570.
Oliet, S.H., and Bourque, C.W. (1993). Mechanosensitive channels transduce osmosensitivity in supraoptic neurons. Nature *364*, 341-343.
Petersen, O.H. (2002). Cation channels: homing in on the elusive CAN channels. Curr Biol *12*, R520-522.
Piet, R., Vargova, L., Sykova, E., Poulain, D.A., and Oliet, S.H. (2004). Physiological contribution of the astrocytic environment of neurons to intersynaptic crosstalk. Proc Natl Acad Sci U S A *101*, 2151-2155.
Pittman, Q.J., Veale, W.L., and Lederis, K. (1982). Central neurohypophyseal peptide pathways: interactions with endocrine and other autonomic functions. Peptides *3*, 515-520.
Pliquett, R.U., Fasshauer, M., Bluher, M., and Paschke, R. (2004). Neurohumoral stimulation in type-2-diabetes as an emerging disease concept. Cardiovasc Diabetol *3*, 4.
Pow, D.V., and Morris, J.F. (1989). Dendrites of hypothalamic magnocellular neurons release neurohypophysial peptides by exocytosis. Neuroscience *32*, 435-439.
Salio, C., Lossi, L., Ferrini, F., and Merighi, A. (2006). Neuropeptides as synaptic transmitters. Cell Tissue Res *326*, 583-598.
Shi, P., Stocker, S.D., and Toney, G.M. (2007). Organum vasculosum laminae terminalis contributes to increased sympathetic nerve activity induced by central hyperosmolality. Am J Physiol Regul Integr Comp Physiol *293*, R2279-2289.
Sonner, P.M., Lee, S., Ryu, P.D., Lee, S.Y., and Stern, J.E. (2011). Imbalanced K+ and Ca2+ subthreshold interactions contribute to increased hypothalamic presympathetic neuronal excitability in hypertensive rats. J Physiol *589*, 667-683.
Swanson, L.W., and Kuypers, H.G. (1980). The paraventricular nucleus of the hypothalamus: cytoarchitectonic subdivisions and organization of projections to the pituitary, dorsal vagal complex, and spinal cord as demonstrated by retrograde fluorescence double-labeling methods. J Comp Neurol *194*, 555-570.
Swanson, L.W., and Sawchenko, P.E. (1980). Paraventricular nucleus: a site for the integration of neuroendocrine and autonomic mechanisms. Neuroendocrinology *31*, 410-417.
Swanson, L.W., Sawchenko, P.E., Wiegand, S.J., and Price, J.L. (1980). Separate neurons in the paraventricular nucleus project to the median eminence and to the medulla or spinal cord. Brain Res *198*, 190-195.
Teruyama, R., and Armstrong, W.E. (2007). Calcium-dependent fast depolarizing afterpotentials in vasopressin neurons in the rat supraoptic nucleus. J Neurophysiol *98*, 2612-2621.

Teruyama, R., Sakuraba, M., Kurotaki, H., and Armstrong, W.E. (2011). Transient receptor potential channel m4 and m5 in magnocellular cells in rat supraoptic and paraventricular nuclei. J Neuroendocrinol *23*, 1204-1213.
Tobin, V.A., Hashimoto, H., Wacker, D.W., Takayanagi, Y., Langnaese, K., Caquineau, C., Noack, J., Landgraf, R., Onaka, T., Leng, G.*, et al.* (2010). An intrinsic vasopressin system in the olfactory bulb is involved in social recognition. Nature *464*, 413-417.
Toney, G.M., and Stocker, S.D. (2010). Hyperosmotic activation of CNS sympathetic drive: implications for cardiovascular disease. J Physiol *588*, 3375-3384.
Ueta, Y., Fujihara, H., Serino, R., Dayanithi, G., Ozawa, H., Matsuda, K.-i., Kawata, M., Yamada, J., Ueno, S., Fukuda, A., and Murphy, D. (2005). Transgenic expression of enhanced green fluorescent protein enables direct visualization for physiological studies of vasopressin neurons and isolated nerve terminals of the rat. Endocrinology *146*, 406-413.
Ullrich, N.D., Voets, T., Prenen, J., Vennekens, R., Talavera, K., Droogmans, G., and Nilius, B. (2005). Comparison of functional properties of the Ca2+-activated cation channels TRPM4 and TRPM5 from mice. Cell Calcium *37*, 267-278.
Xu, H.L., Mao, L., Ye, S., Paisansathan, C., Vetri, F., and Pelligrino, D.A. (2008). Astrocytes are a key conduit for upstream signaling of vasodilation during cerebral cortical neuronal activation in vivo. Am J Physiol Heart Circ Physiol *294*, H622-632.
Zingg, H.H. (1996). Vasopressin and oxytocin receptors. Baillieres Clin Endocrinol Metab *10*, 75-96.

Figure 1
Click here to download high resolution image

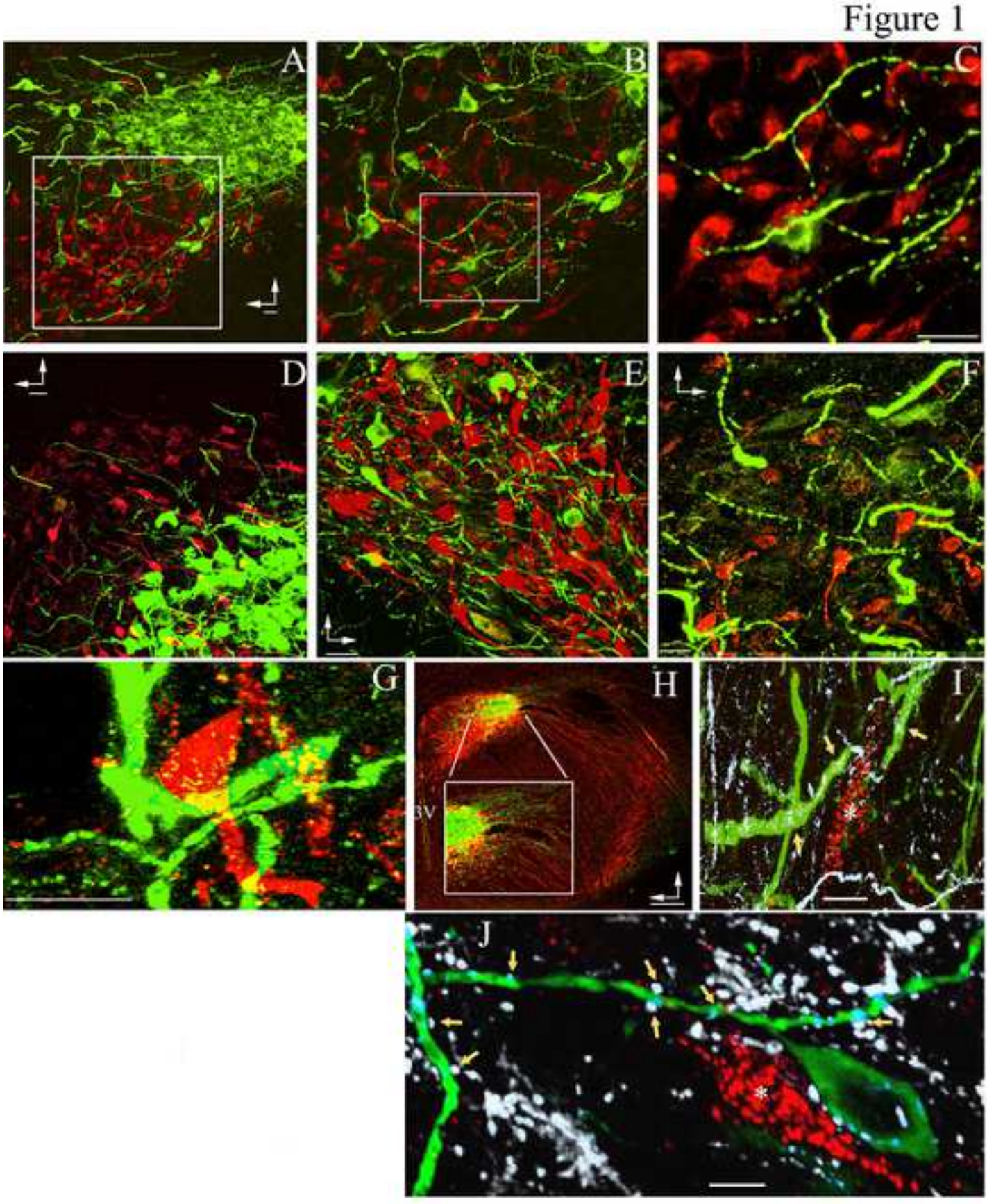

Figure 2

Click here to download high resolution image

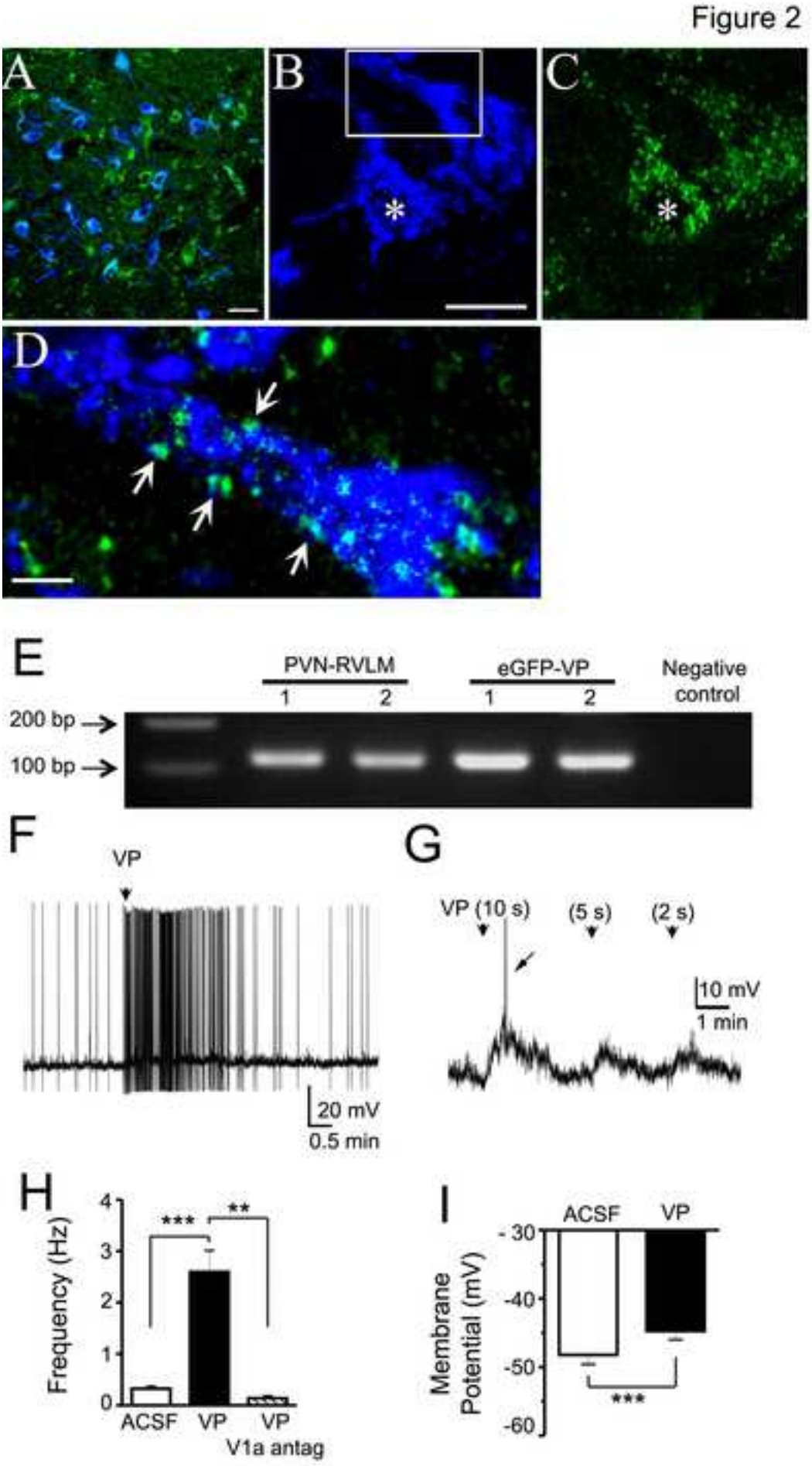

Figure 3
Click here to download high resolution image

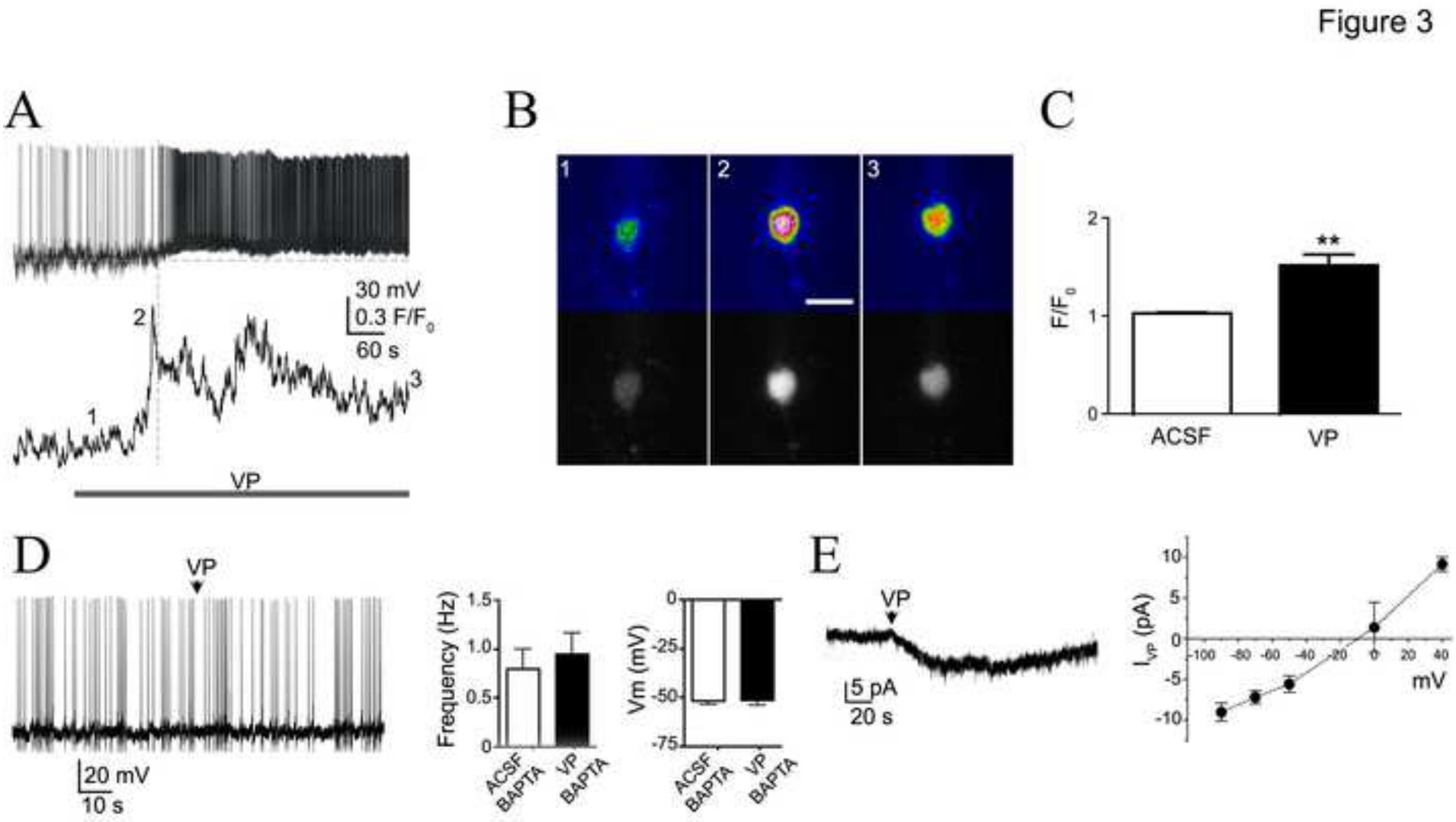

Figure 4

Click here to download high resolution image

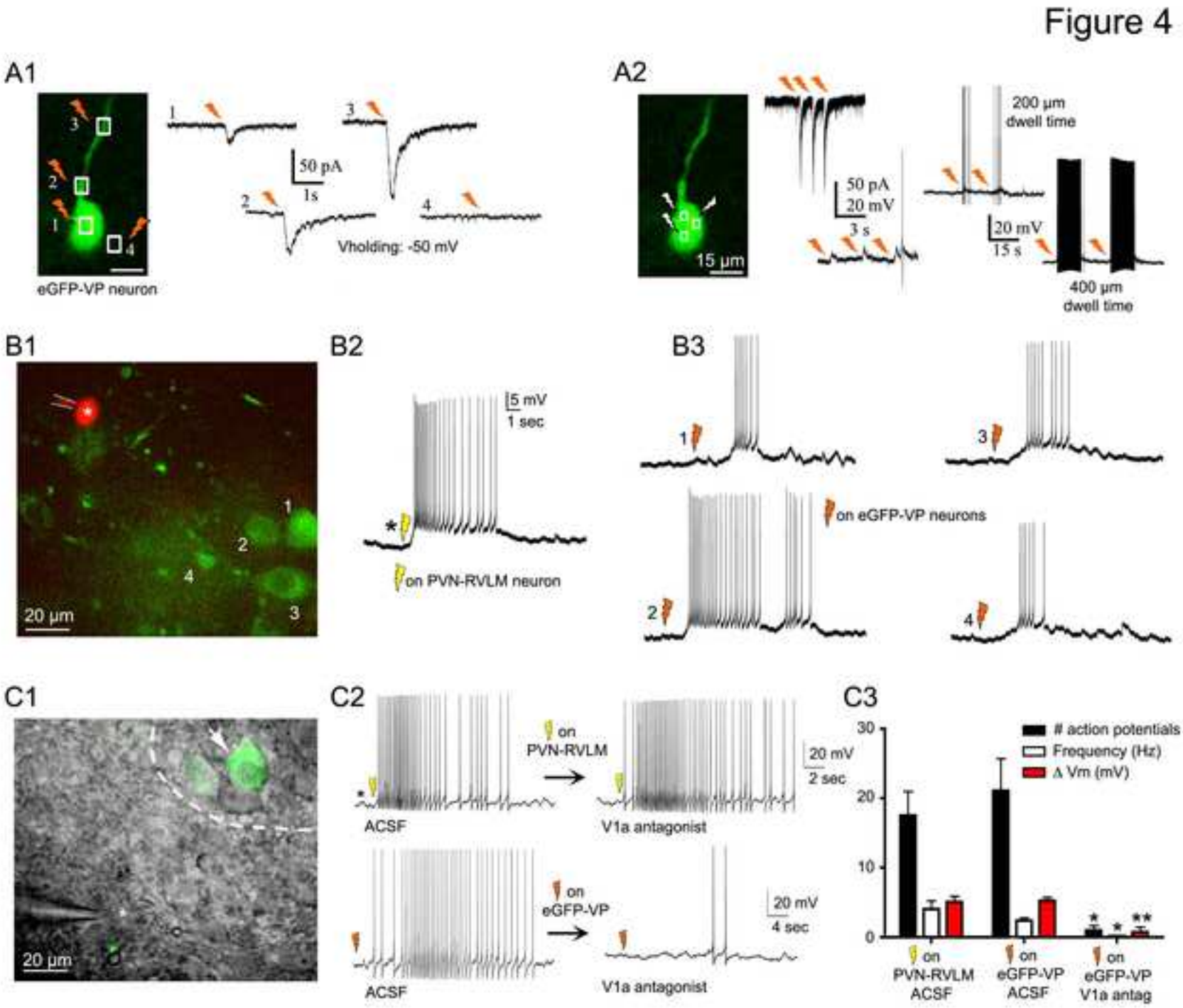

Figure 5
Click here to download high resolution image

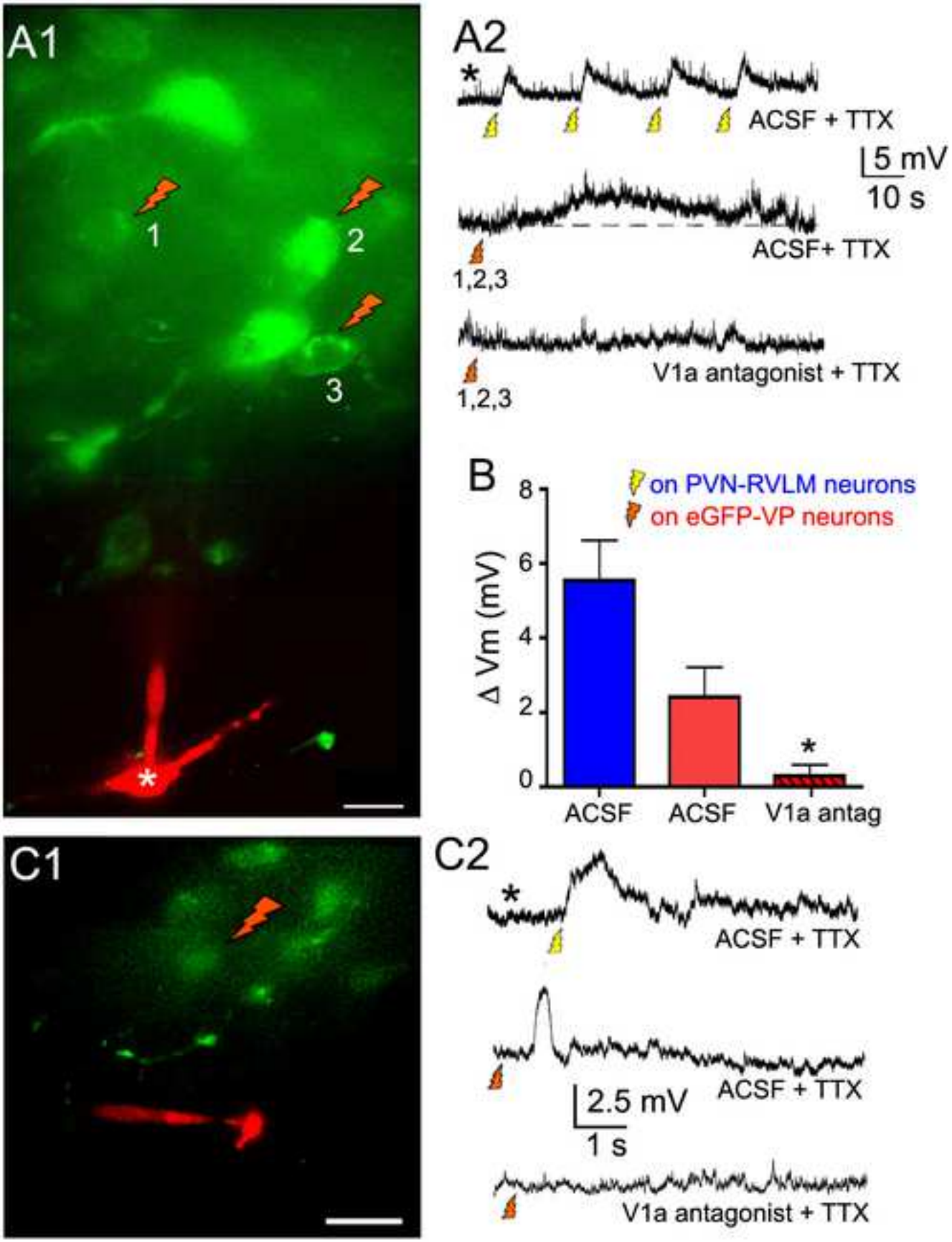

Figure 6
Click here to download high resolution image

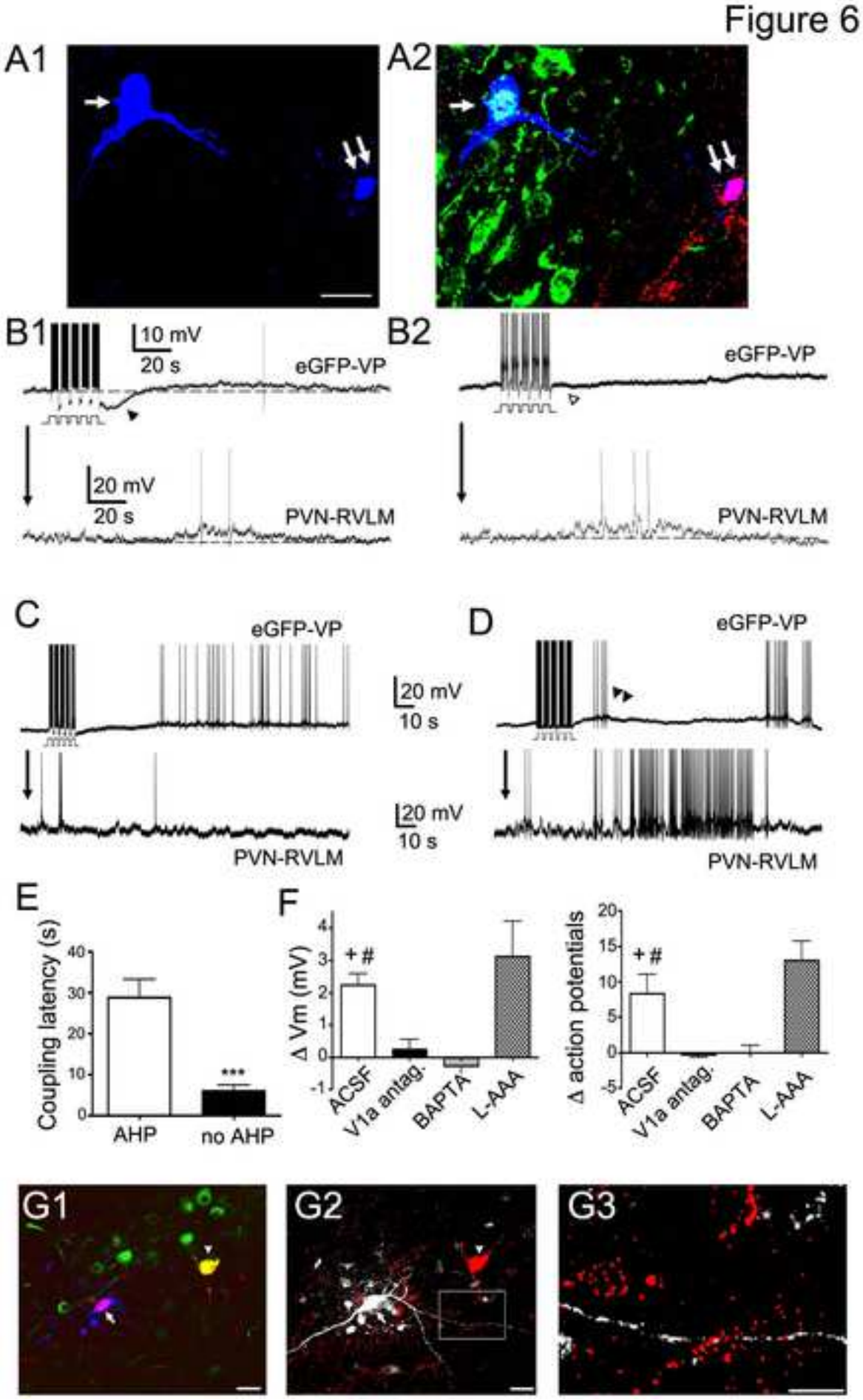

Figure 7

Click here to download high resolution image

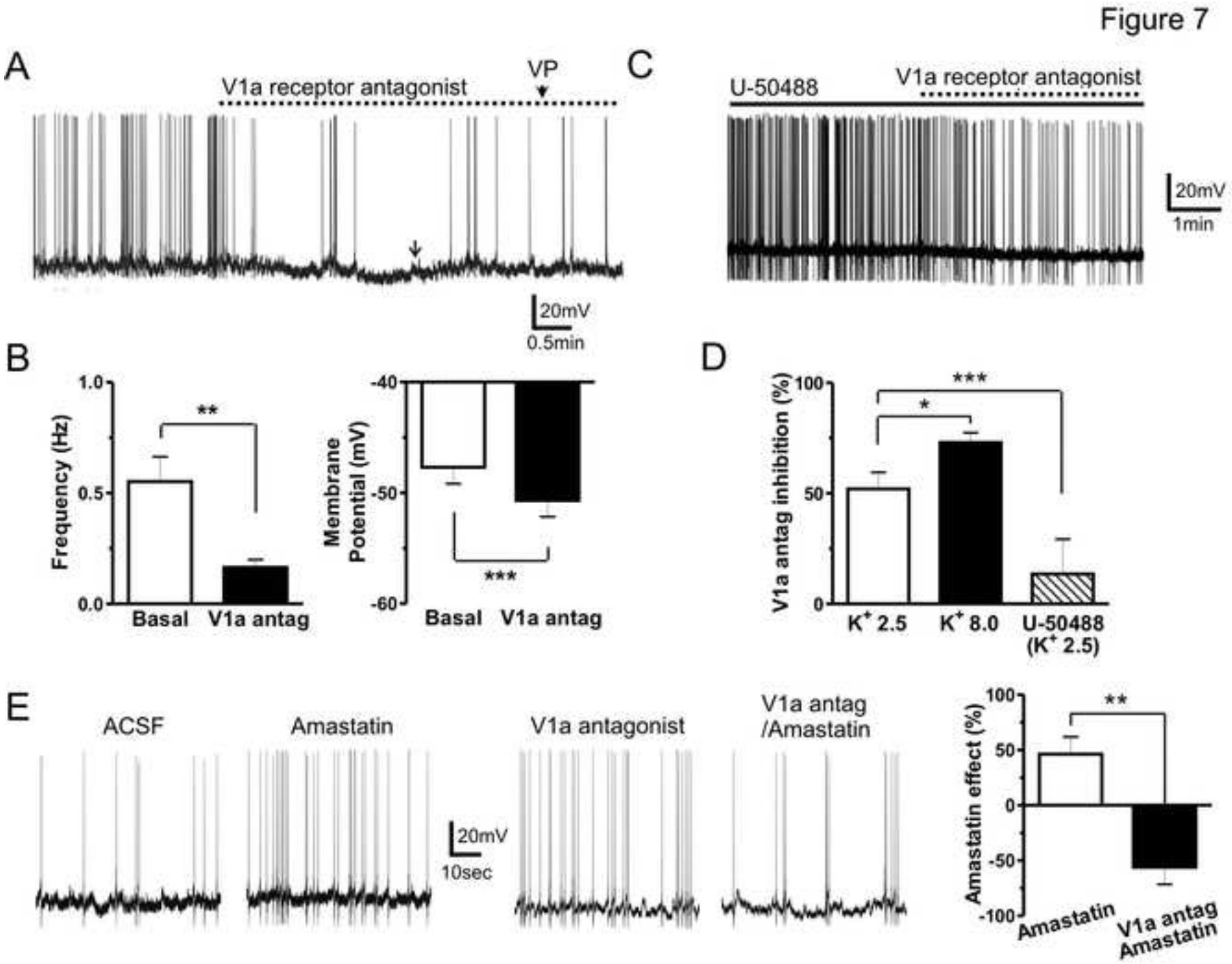

Figure 8
Click here to download high resolution image